



TECH BRIEFS

NATIONAL AERONAUTICS AND SPACE ADMINISTRATION

-  **Technology Focus**
-  **Electronics/Computers**
-  **Software**
-  **Materials**
-  **Mechanics/Machinery**
-  **Manufacturing**
-  **Bio-Medical**
-  **Physical Sciences**
-  **Information Sciences**
-  **Books and Reports**

INTRODUCTION

Tech Briefs are short announcements of innovations originating from research and development activities of the National Aeronautics and Space Administration. They emphasize information considered likely to be transferable across industrial, regional, or disciplinary lines and are issued to encourage commercial application.

Availability of NASA Tech Briefs and TSPs

Requests for individual Tech Briefs or for Technical Support Packages (TSPs) announced herein should be addressed to

National Technology Transfer Center

Telephone No. (800) 678-6882 or via World Wide Web at www2.nttc.edu/leads/

Please reference the control numbers appearing at the end of each Tech Brief. Information on NASA's Innovative Partnerships Program (IPP), its documents, and services is also available at the same facility or on the World Wide Web at <http://ipp.nasa.gov>.

Innovative Partnerships Offices are located at NASA field centers to provide technology-transfer access to industrial users. Inquiries can be made by contacting NASA field centers listed below.

NASA Field Centers and Program Offices

Ames Research Center

Lisa L. Lockyer
(650) 604-1754
lisa.l.lockyer@nasa.gov

Dryden Flight Research Center

Gregory Poteat
(661) 276-3872
greg.poteat@dfrc.nasa.gov

Glenn Research Center

Kathy Needham
(216) 433-2802
kathleen.k.needham@nasa.gov

Goddard Space Flight Center

Nona Cheeks
(301) 286-5810
nona.k.cheeks@nasa.gov

Jet Propulsion Laboratory

Ken Wolfenbarger
(818) 354-3821
james.k.wolfenbarger@jpl.nasa.gov

Johnson Space Center

Michele Brekke
(281) 483-4614
michele.a.brekke@nasa.gov

Kennedy Space Center

David R. Makufka
(321) 867-6227
david.r.makufka@nasa.gov

Langley Research Center

Martin Waszak
(757) 864-4015
martin.r.waszak@nasa.gov

Marshall Space Flight Center

Jim Dowdy
(256) 544-7604
jim.dowdy@msfc.nasa.gov

Stennis Space Center

John Bailey
(228) 688-1660
john.w.bailey@nasa.gov

Carl Ray, Program Executive

Small Business Innovation
Research (SBIR) & Small
Business Technology
Transfer (STTR) Programs
(202) 358-4652
carl.g.ray@nasa.gov

Doug Comstock, Director

Innovative Partnerships
Program Office
(202) 358-2560
doug.comstock@nasa.gov



TECH BRIEFS

NATIONAL AERONAUTICS AND SPACE ADMINISTRATION



5 Technology Focus: Communications

- 5 Miniature Intelligent Sensor Module
- 5 "Smart" Sensor Module
- 6 Portable Apparatus for Electrochemical Sensing of Ethylene
- 7 Increasing Linear Dynamic Range of a CMOS Image Sensor
- 8 Flight Qualified Micro Sun Sensor



9 Materials

- 9 Norbornene-Based Polymer Electrolytes for Lithium Cells
- 10 Making Single-Source Precursors of Ternary Semiconductors
- 10 Water-Free Proton-Conducting Membranes for Fuel Cells



13 Electronics/Computers

- 13 Mo/Ti Diffusion Bonding for Making Thermoelectric Devices
- 14 Photodetectors on Coronagraph Mask for Pointing Control
- 14 High-Energy-Density, Low-Temperature Li/CFx Primary Cells
- 15 G₄-FETs as Universal and Programmable Logic Gates



17 Manufacturing & Prototyping

- 17 Fabrication of Buried Nanochannels From Nanowire Patterns
- 17 Diamond Smoothing Tools



19 Bio-Medical

- 19 Infrared Imaging System for Studying Brain Function



21 Physical Sciences

- 21 Rarefying Spectra of Whispering-Gallery-Mode Resonators
- 22 Large-Area Permanent-Magnet ECR Plasma Source
- 22 Slot-Antenna/Permanent-Magnet Device for Generating Plasma
- 23 Fiber-Optic Strain Gauge With High Resolution And Update Rate
- 23 Broadband Achromatic Telecentric Lens



25 Information Sciences

- 25 Temperature-Corrected Model of Turbulence in Hot Jet Flows
- 26 Enhanced Elliptic Grid Generation
- 26 Automated Knowledge Discovery From Simulators
- 27 Electro-Optical Modulator Bias Control Using Bipolar Pulses
- 28 Generative Representations for Automated Design of Robots



30 Books & Reports

- 30 Mars-Approach Navigation Using In Situ Orbiters
- 30 Efficient Optimization of Low-Thrust Spacecraft Trajectories
- 30 Cylindrical Asymmetrical Capacitors for Use in Outer Space
- 30 Protecting Against Faults in JPL Spacecraft
- 31 Algorithm Optimally Allocates Actuation of a Spacecraft
- 31 Radar Interferometer for Topographic Mapping of Glaciers and Ice Sheets

This document was prepared under the sponsorship of the National Aeronautics and Space Administration. Neither the United States Government nor any person acting on behalf of the United States Government assumes any liability resulting from the use of the information contained in this document, or warrants that such use will be free from privately owned rights.



Miniature Intelligent Sensor Module

This unit performs signal-conditioning, data-processing, and health-monitoring functions.

Stennis Space Center, Mississippi

An electronic unit denoted the Miniature Intelligent Sensor Module performs sensor-signal-conditioning functions and local processing of sensor data. The unit includes four channels of analog input/output circuitry, a processor, volatile and nonvolatile memory, and two Ethernet communication ports, all housed in a weathertight enclosure. The unit accepts AC or DC power. The analog inputs provide programmable gain, offset, and filtering as well as shunt calibration and auto-zeroing. Analog outputs include sine, square, and triangular waves having programmable frequencies and amplitudes, as well as programmable amplitude DC.

One innovative aspect of the design of this unit is the integration of a relatively powerful processor and large amount of memory along with the sensor-signal-

conditioning circuitry so that sophisticated computer programs can be used to acquire and analyze sensor data and estimate and track the “health” of the overall sensor-data-acquisition system of which the unit is a part. The unit includes calibration, zeroing, and signal-feedback circuitry to facilitate health monitoring. The processor is also integrated with programmable logic circuitry in such a manner as to simplify and enhance acquisition of data and generation of analog outputs.

A notable unique feature of the unit is a cold-junction compensation circuit in the back shell of a sensor connector. This circuit makes it possible to use K-type thermocouples without compromising a housing seal.

Replicas of this unit may prove useful in industrial and manufacturing settings

— especially in such large outdoor facilities as refineries. Two features can be expected to simplify installation: the weathertight housings should make it possible to mount the units near sensors, and the Ethernet communication capability of the units should facilitate establishment of communication connections for the units.

This work was done by Russell S. Beech of NVE Corp. for Stennis Space Center.

Inquiries concerning rights for the commercial use of this invention should be addressed to:

NVE Corporation

11409 Valley View Road

Eden Prairie, MN 55344-3617

(952) 996-1602

E-mail: beech@nve.com

Refer to SSC-00246, volume and number of this NASA Tech Briefs issue, and the page number.

“Smart” Sensor Module

This is a prototype building block of advanced engineering-health-monitoring systems.

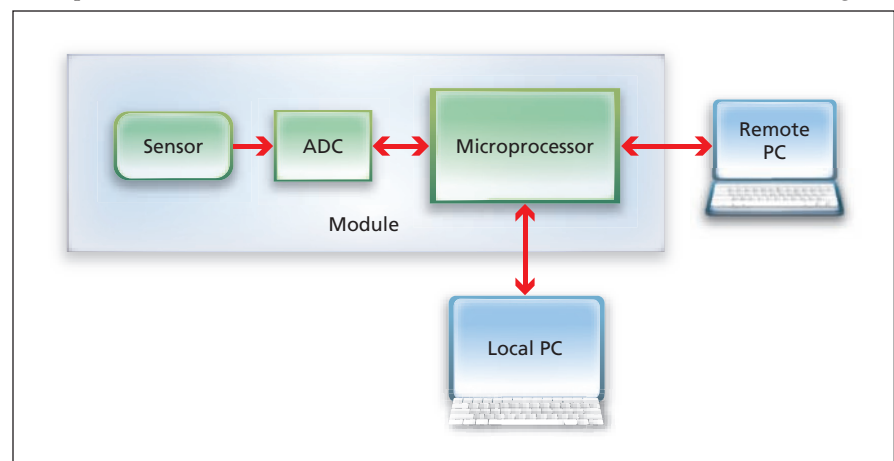
Stennis Space Center, Mississippi

An assembly that contains a sensor, sensor-signal-conditioning circuitry, a sensor-readout analog-to-digital converter (ADC), data-storage circuitry, and a microprocessor that runs special-purpose software and communicates with one or more external computer(s) has been developed as a prototype of “smart” sensor modules for monitoring the integrity and functionality (the “health”) of engineering systems. Although these modules are now being designed specifically for use on rocket-engine test stands, it is anticipated that they could also readily be designed to be incorporated into health-monitoring subsystems of such diverse engineering systems as spacecraft, aircraft, land vehicles, bridges, buildings, power plants, oilrigs, and defense installations.

The figure is a simplified block diagram of the “smart” sensor module. The analog sensor readout signal is

processed by the ADC, the digital output of which is fed to the microprocessor. By means of a standard RS-232 cable, the microprocessor is connected to a local

personal computer (PC), from which software is downloaded into a random-access memory in the microprocessor. The local PC is also used to debug the



The “Smart” Sensor Module is programmed by use of the local PC and thereafter operated by the remote PC. In addition to preprocessed sensory data, the module generates an indication of the reliability of the data (and, hence, of the health of the sensor).

software. Once the software is running, the local PC is disconnected and the module is controlled by, and all output data from the module are collected by, a remote PC via an Ethernet bus. Several "smart" sensor modules like this one could be connected to the same Ethernet bus and controlled by the single remote PC.

The software running in the microprocessor includes driver programs for operation of the sensor, programs that implement self-assessment algorithms, programs that implement protocols for communication with the external computer(s), and programs that implement evolutionary methodologies to enable the module to improve its performance

over time. The design of the module and of the health-monitoring system of which it is a part reflects the understanding that the main purpose of a health-monitoring system is to detect damage and, therefore, the health-monitoring system must be able to function effectively in the presence of damage and should be capable of distinguishing between damage to itself and damage to the system being monitored. A major benefit afforded by the self-assessment algorithms is that in the output of the module, the sensor data indicative of the health of the engineering system being monitored are coupled with a confidence factor that quantifies the degree of reliability of the data. Hence, the output includes information on the

health of the sensor module itself in addition to information on the health of the engineering system being monitored.

This work was done by Ajay Mahajan of Southern Illinois University for Stennis Space Center.

Inquiries concerning rights for its commercial use should be addressed to:

*Southern Illinois University at Carbondale
Department of Mechanical Engineering
and Energy Processes*

Carbondale, IL 62901

Attn: Dr. Ajay Mahajan

(618)453-7007

mahajan@engr.siu.edu

Refer to SSC-00242, volume and number of this NASA Tech Briefs issue, and the page number.

Portable Apparatus for Electrochemical Sensing of Ethylene

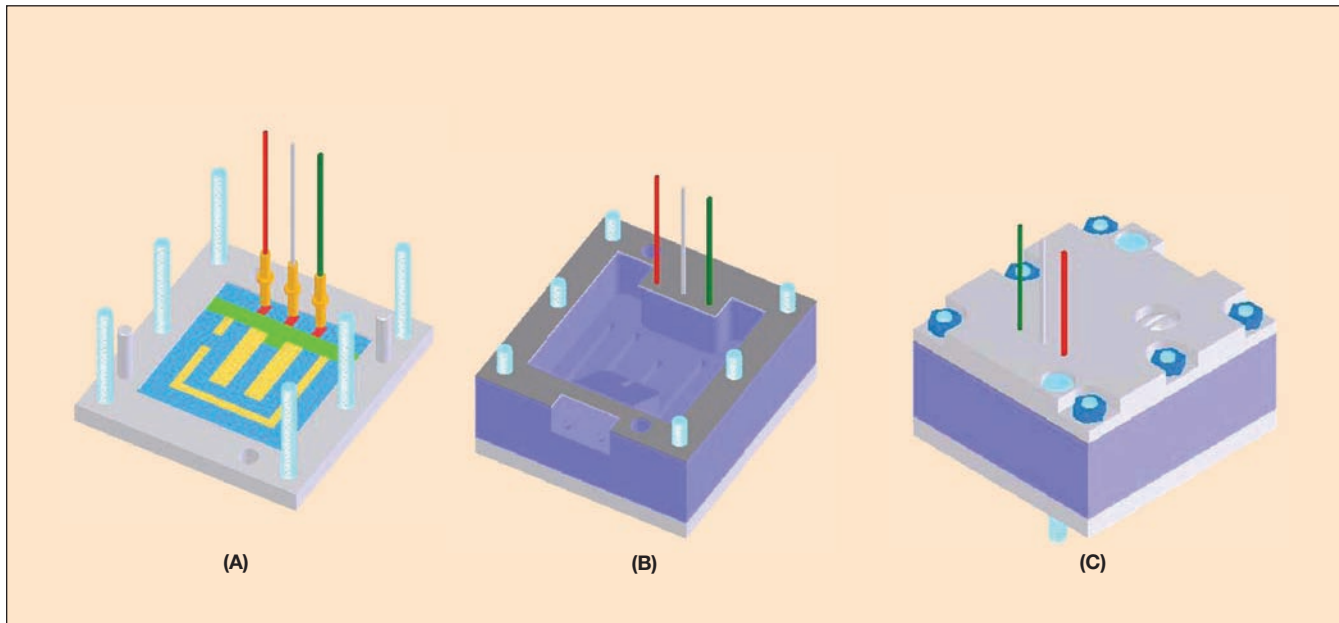
Concentrations between 5 and 5,000 ppb can be measured.

John F. Kennedy Space Center, Florida

A small, lightweight, portable apparatus based on an electrochemical sensing principle has been developed for monitoring low concentrations of ethylene in air. Ethylene has long been known to be produced by plants and to stimulate the growth and other aspects of the development of plants (including, notably, ripening of fruits and vegetables), even at concentrations as low as tens of parts per billion (ppb). The effects are magni-

fied in plant-growth and -storage chambers wherein ethylene can accumulate. There is increasing recognition in agriculture and related industries that it is desirable to monitor and control ethylene concentrations in order to optimize the growth, storage, and ripening of plant products. Hence, there are numerous potential uses for the present apparatus in conjunction with equipment for controlling ethylene concentrations.

The ethylene sensor is of a thick-film type with a design optimized for a low detection limit. The sensor includes a noble metal sensing electrode on a chip and a hydrated solid-electrolyte membrane that is held in contact with the chip. Also located on the sensor chip are a counter electrode and a reference electrode. The sensing electrode is held at a fixed potential versus the reference electrode. Detection takes place at ac-



The **Sensor Chip and Solid-Electrolyte Membrane** are packaged together in a housing that contains airflow channels and a reservoir for water to keep the membrane wet. In the illustrated design, (A) the sensor chip is shown in its holder with its three electrical lead pins and (B) the upper portion of the sensor housing is shown with the water reservoir and slots to hydrate Nafion (or equivalent) membrane, which is placed over the sensor chip. The assembled sensor ready for installation in the ethylene monitor is shown in (C). It measures 4 by 4 by 2.2 cm.

tive-triple-point areas where the sensing electrode, electrolyte, and sample gas meet. These areas are formed by cutting openings in the electrolyte membrane. The electrode current generated from electrochemical oxidation of ethylene at the active triple points is proportional to the concentration of ethylene. An additional film of the solid-electrolyte membrane material is deposited on the sensing electrode to increase the effective triple-point areas and thereby enhance the detection signal.

The sensor chip is placed in a holder that is part of a polycarbonate housing. When fully assembled, the housing holds the solid-electrolyte membrane in contact with the chip (see figure). The housing includes a water reservoir for keeping the solid-electrolyte membrane hydrated. The housing also includes flow channels for circulating a sample stream of air over the chip: ethylene is brought to the sensing surface predom-

inately by convection in this sample stream. The sample stream is generated by a built-in sampling pump. The forced circulation of sample air contributes to the attainment of a low detection limit.

In addition to the sensor and the sampling pump, the apparatus includes electronic circuitry for regulating the sensor potentials, measuring the sensing-electrode current, and displaying the ethylene-concentration reading. The electronic circuitry includes a data logger for digital collection via a serial port with an optional analog output.

Overall, the apparatus is capable of measuring ethylene concentrations from 5 to 5,000 ppb with a response time of less than 30 seconds. The magnitude of response of the sensor current is in the range of 5 to 50 picoamperes/ppb. The signal-to-noise ratio is greater than 3 at the low detection limit of 5 ppb.

The sensor is fairly selective for ethylene. It is not subject to interference by O_2 or CO_2 . It does respond to NO , NO_2 , and H_2S , but these gases are generally not expected to be present at significant concentrations in controlled plant-growth environments. The sensor also responds to some volatile compounds present in some soil samples. Further research will be necessary to reduce these interferences.

This work was done by Mourad Manoukian, Linda A. Tempelman, and John Forchione of Giner, Inc. and W. Michael Krebs and Edwin W. Schmitt of Giner Electrochemical Systems, LLC for Kennedy Space Center. For further information, contact:

*Linda A. Tempelman, Ph.D.
Giner, Inc.
89 Rumford Ave.
Newton, MA 02466
Phone No.: (781) 529-0514
E-mail: ltempelman@ginerinc.com
Refer to KSC-12825.*

Increasing Linear Dynamic Range of a CMOS Image Sensor

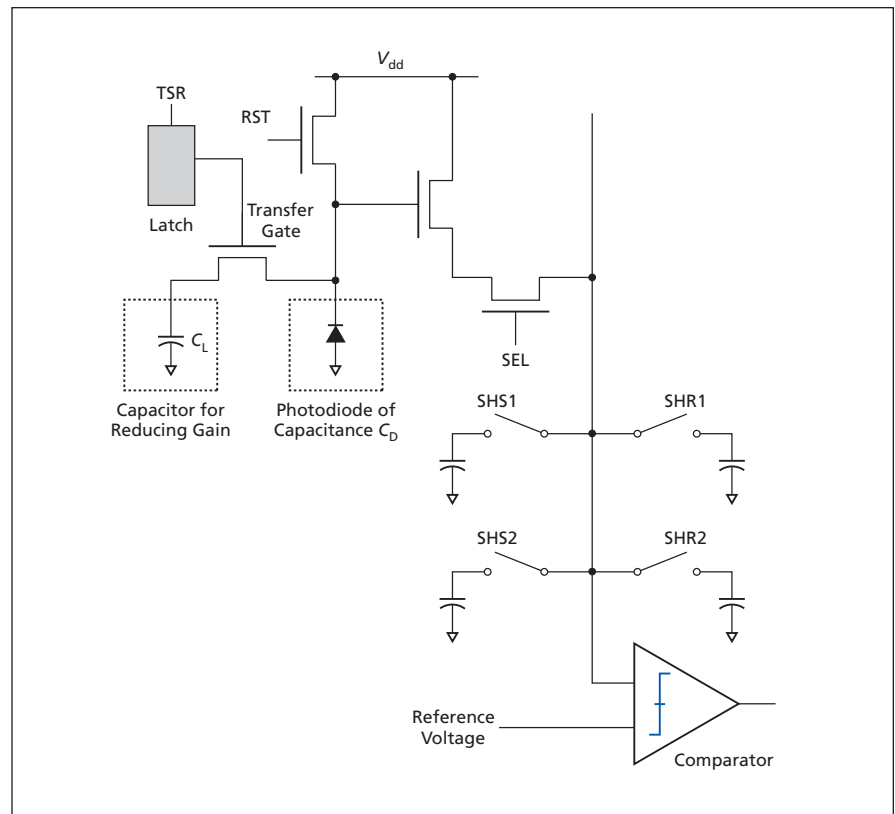
Dual-gain pixels are automatically switched to the most appropriate gain level.

NASA's Jet Propulsion Laboratory, Pasadena, California

A generic design and a corresponding operating sequence have been developed for increasing the linear-response dynamic range of a complementary metal oxide/semiconductor (CMOS) image sensor. The design provides for linear calibrated dual-gain pixels that operate at high gain at a low signal level and at low gain at a signal level above a preset threshold. Unlike most prior designs for increasing dynamic range of an image sensor, this design does not entail any increase in noise (including fixed-pattern noise), decrease in responsivity or linearity, or degradation of photometric calibration.

The figure is a simplified schematic diagram showing the circuit of one pixel and pertinent parts of its column readout circuitry. The conventional part of the pixel circuit includes a photodiode having a small capacitance, C_D . The unconventional part includes an additional larger capacitance, C_L , that can be connected to the photodiode via a transfer gate controlled in part by a latch.

In the high-gain mode, the signal labeled TSR in the figure is held low through the latch, which also helps to adapt the gain on a pixel-by-pixel basis.



The Pixel and Column Readout Circuitry enable operation in either of two gain modes and automatic choice of whichever mode is appropriate for the present illumination level.

Light must be coupled to the pixel through a microlens or by back illumination in order to obtain a high effective fill factor; this is necessary to ensure high quantum efficiency, a loss of which would minimize the efficacy of the dynamic-range-enhancement scheme. Once the level of illumination of the pixel exceeds the threshold, TSR is turned on, causing the transfer gate to conduct, thereby adding C_t to the pixel capacitance. The added capacitance reduces the conversion gain, and increases the pixel electron-handling capacity, thereby providing an extension of the dynamic range.

By use of an array of comparators also at the bottom of the column, photocharge voltages on sampling capacitors in each column are compared with

a reference voltage to determine whether it is necessary to switch from the high-gain to the low-gain mode. Depending upon the built-in offset in each pixel and in each comparator, the point at which the gain change occurs will be different, adding gain-dependent fixed pattern noise in each pixel. The offset, and hence the fixed pattern noise, is eliminated by sampling the pixel readout charge four times by use of four capacitors (instead of two such capacitors as in conventional design) connected to the bottom of the column via electronic switches SHS1, SHR1, SHS2, and SHR2, respectively, corresponding to high and low values of the signals TSR and RST. The samples are combined in an appropriate fashion to cancel offset-induced errors, and provide spurious-free imag-

ing with extended dynamic range.

This work was done by Bedabrata Pain of Caltech for NASA's Jet Propulsion Laboratory. Further information is contained in a TSP (see page 1).

In accordance with Public Law 96-517, the contractor has elected to retain title to this invention. Inquiries concerning rights for its commercial use should be addressed to:

*Innovative Technology Assets Management
JPL*

*Mail Stop 202-233
4800 Oak Grove Drive
Pasadena, CA 91109-8099
(818) 354-2240*

E-mail: iaoffice@jpl.nasa.gov

Refer to NPO-41897, volume and number of this NASA Tech Briefs issue, and the page number.

Flight Qualified Micro Sun Sensor

Attributes include compactness, low mass, and low power consumption.

NASA's Jet Propulsion Laboratory, Pasadena, California

A prototype small, lightweight micro Sun sensor (MSS) has been flight qualified as part of the attitude-determination system of a spacecraft or for Mars surface operations. The MSS has previously been reported at a very early stage of development in *NASA Tech Briefs*, Vol. 28, No. 1 (January 2004).

An MSS is essentially a miniature multiple-pinhole electronic camera combined with digital processing electronics that functions analogously to a sundial. A micromachined mask containing a number of microscopic pinholes is mounted in front of an active-pixel sen-

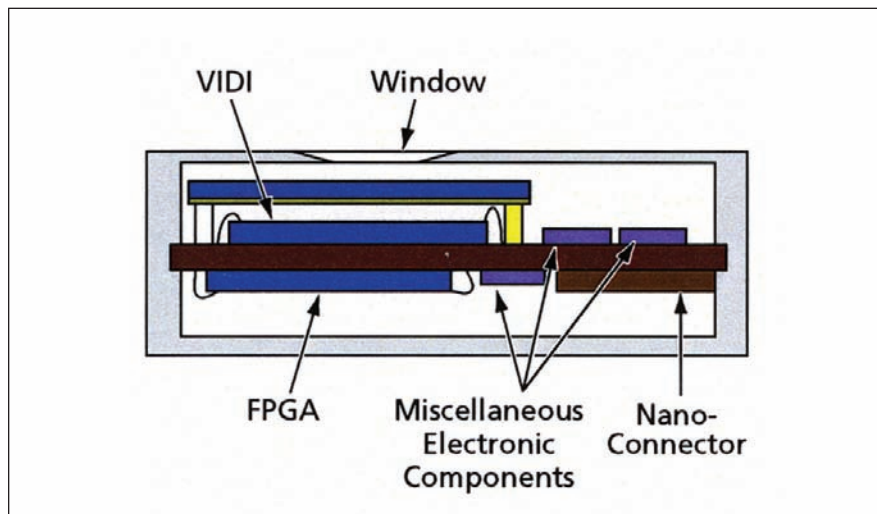
sor (APS). Electronic circuits for controlling the operation of the APS, readout from the pixel photodetectors, and analog-to-digital conversion are all integrated onto the same chip along with the APS. The digital processing includes computation of the centroids of the pinhole Sun images on the APS. The spacecraft computer has the task of converting the Sun centroids into Sun angles utilizing a calibration polynomial.

The micromachined mask comprises a 500- μm -thick silicon wafer, onto which is deposited a 57-nm-thick chromium adhesion-promotion layer followed by a

200-nm-thick gold light-absorption layer. The pinholes, 50 μm in diameter, are formed in the gold layer by photolithography. The chromium layer is thin enough to be penetrable by an amount of Sunlight adequate to form measurable pinhole images. A spacer frame between the mask and the APS maintains a gap of ≈ 1 mm between the pinhole plane and the photodetector plane of the APS.

To minimize data volume, mass, and power consumption, the digital processing of the APS readouts takes place in a single field-programmable gate array (FPGA). The particular FPGA is a radiation-tolerant unit that contains $\approx 32,000$ gates. No external memory is used so the FPGA calculates the centroids in real time as pixels are read off the APS with minimal internal memory. To enable the MSS to fit into a small package, the APS, the FPGA, and other components are mounted on a single two-sided board following chip-on-board design practices (see figure).

*This work was done by Carl Christian Liebe, Sohrab Mobasser, Chris Wrigley, Jeffrey Schroeder, Youngsam Bae, James Naegle, Sunant Katanyoutanant, Sergei Jerebets, Donald Schatzel, and Choonsup Lee of Caltech for NASA's Jet Propulsion Laboratory. Further information is contained in a TSP (see page 1).
NPO-43620*



The Entire MSS fits into a compact package.



Norbornene-Based Polymer Electrolytes for Lithium Cells

These solid electrolytes are single-ion conductors.

NASA's Jet Propulsion Laboratory, Pasadena, California

Norbornene-based polymers have shown promise as solid electrolytes for lithium-based rechargeable electrochemical cells. These polymers are characterized as single-ion conductors.

Single-ion-conducting polymers that can be used in lithium cells have long been sought. Single-ion conductors are preferred to multiple-ion conductors as solid electrolytes because concentration gradients associated with multiple-ion conduction lead to concentration polarization. By minimizing concentration polarization, one can enhance charge and discharge rates.

Norbornene sulfonic acid esters have been synthesized by a ring-opening metathesis polymerization technique, using ruthenium-based catalysts. The resulting polymer structures (see figure) include sulfonate ionomers attached to the backbones of the polymer molecules. These molecules are single-ion conductors in that they conduct mobile

Li⁺ ions only; the —SO₃⁻ anions in these polymers, being tethered to the backbones, do not contribute to ionic conduction.

This molecular system is especially attractive in that it is highly amenable to modification through functionalization of the backbone or copolymerization with various monomers. Polymers of this type have been blended with poly(ethylene oxide) to lend mechanical integrity to free-standing films, and the films have been fabricated into solid polymer electrolytes. These electrolytes have been demonstrated to exhibit conductivity of 2×10^{-5} S·cm (which is high, relative to the conductivities of other solid electrolytes) at ambient temperature, plus acceptably high stability.

This type of norbornene-based polymeric solid electrolyte is in the early stages of development. Inasmuch as the method of synthesis of these polymers is inherently flexible and techniques for

the fabrication of the polymers into solid electrolytes are amenable to optimization, there is reason to anticipate further improvements.

This work was done by Iris Cheung and Marshall Smart of Caltech and Surya Prakash, Akira Miyazawa, and Jinbo Hu of the University of Southern California for NASA's Jet Propulsion Laboratory. Further information is contained in a TSP (see page 1).

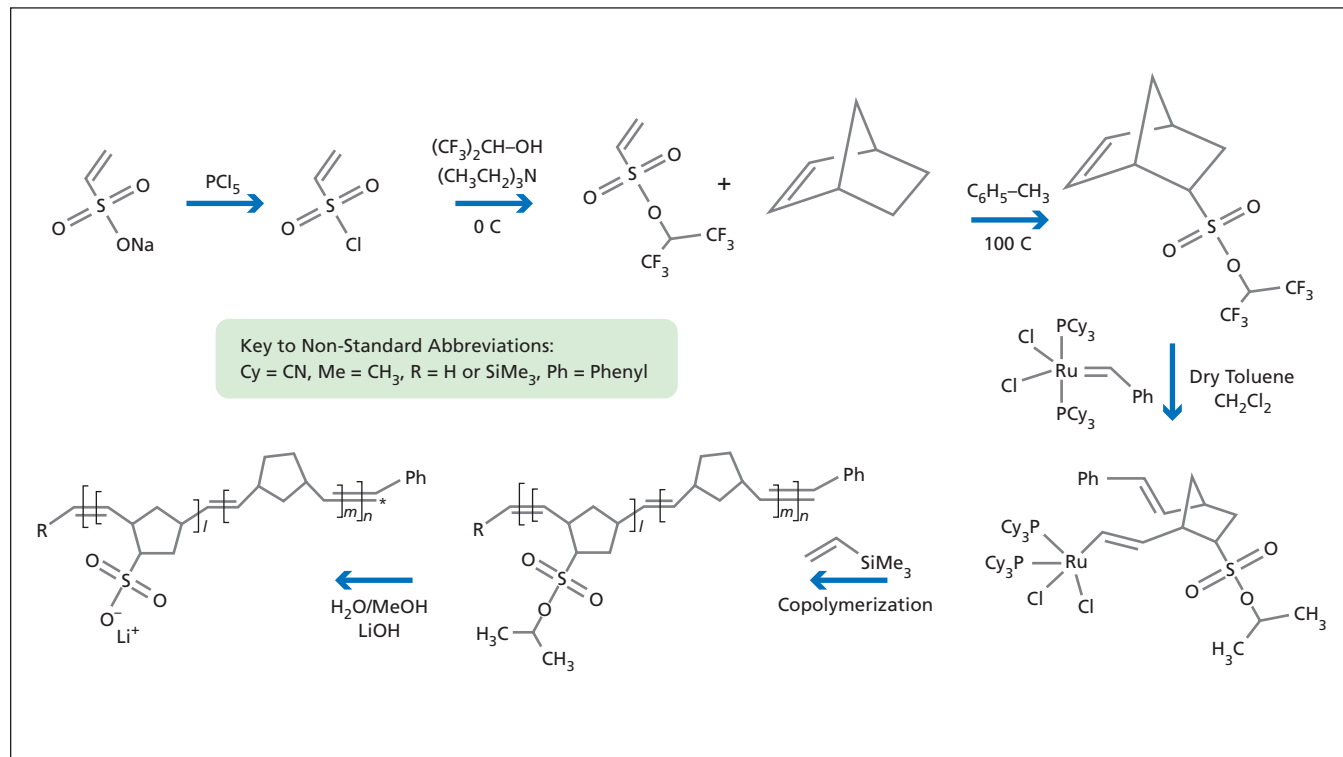
In accordance with Public Law 96-517, the contractor has elected to retain title to this invention. Inquiries concerning rights for its commercial use should be addressed to:

*Innovative Technology Assets Management
JPL*

*Mail Stop 202-233
4800 Oak Grove Drive
Pasadena, CA 91109-8099
(818) 354-2240*

E-mail: iaoffice@jpl.nasa.gov

Refer to NPO-41134, volume and number of this NASA Tech Briefs issue, and the page number.



This Sequence of Reactions yields a cyclopentane-based polymer structure that includes sulfonate ionomers attached to the backbones. Li⁺ ions are loosely bound to the sulfonate ionomers.

◆ Making Single-Source Precursors of Ternary Semiconductors

Commercially available reagents are used in a simplified synthesis.

John H. Glenn Research Center, Cleveland, Ohio

A synthesis route has been developed for the commercial manufacture of single-source precursors of chalcopyrite semiconductor absorber layers of thin-film solar photovoltaic cells. The semiconductors in question are denoted by the general formula $\text{CuIn}_x\text{Ga}_{1-x}\text{S}_y\text{Se}_{2-y}$, where $0 \leq x \leq 1$ and $0 \leq y \leq 1$.

A closely related class of single-source precursors of these semiconductors, and their synthesis routes, were reported in "Improved Single-Source Precursors for Solar-Cell Absorbers" (LEW-17445-1), *NASA Tech Briefs*, Vol. 31, No. 6 (June 2007), page 56. Heretofore, the synthesis of single-source precursors of $\text{CuIn}_x\text{Ga}_{1-x}\text{S}_y\text{Se}_{2-y}$ has involved expensive and/or non-commodity starting reagents and cumbersome, lengthy processes — suitable for laboratory settings but not for commercialization. The present synthesis route is better suited to commercialization because it is simpler and involves the use of commercially available agents, yet offers the flexibil-

ity needed for synthesis of a variety of precursors.

A single-source precursor of the type of interest here is denoted by the general formula $\text{L}_2\text{M}'(\mu\text{-ER})_2\text{M}(\text{ER})_2$, where L signifies a Lewis base; M signifies Al, In, or Ga; M' signifies Ag or Cu; R signifies an alkyl, aryl, silyl, or perfluorocarbon group; E signifies O, S, Se, or Te; and μ signifies a bridging ligand. This compound can be synthesized in a "one-pot" procedure from ingredients that are readily available from almost any chemical supplier. The synthesis of this compound can be summarized in simplified form as $\text{MX}_3 + 4\text{NaER} + \text{M}'\text{X} + 2\text{L} \rightarrow \text{L}_2\text{M}'(\mu\text{-ER})_2\text{M}(\text{ER})_2$, where X signifies a halogen.

In a demonstration, the following synthesis was performed: Under anaerobic conditions, InCl_3 was reacted with sodium ethanethiolate in methanol in a 1:4 molar ratio to afford the ionic stable intermediate compound $\text{Na}^+[\text{In}(\text{SEt})_4]^-$ (where Et signifies ethyl group). After approximately 15 minutes, a heterogeneous solution of CuCl and the Lewis

base PPh_3 (where Ph signifies phenyl) in a 1:2 ratio in a mixture of CH_3CN and CH_2Cl_2 was added directly to the freshly prepared $\text{Na}^+[\text{In}(\text{SEt})_4]^-$. After 24 hours, the reaction was essentially complete. The methanolic solution was concentrated, then the product was extracted with CH_2Cl_2 , then the product was washed with dry ether and pentane. The product in its final form was a creamy white solid. Spectroscopic and elemental analysis confirmed that the product was $(\text{PPh}_3)_2\text{Cu}(\mu\text{-SEt})_2\text{In}(\mu\text{-SEt})_2$, which is known to be a precursor of the ternary semiconductor CuInS_2 .

This work was done by Aloysius Hepp of Glenn Research Center and Kulbinder K. Banger of the Ohio Aerospace Institute. Further information is contained in a TSP (see page 1).

Inquiries concerning rights for the commercial use of this invention should be addressed to NASA Glenn Research Center, Innovative Partnerships Office, Attn: Steve Fedor, Mail Stop 4-8, 21000 Brookpark Road, Cleveland, Ohio 44135. Refer to LEW-17625.

◆ Water-Free Proton-Conducting Membranes for Fuel Cells

Fuel cells could be operated at higher temperatures for greater efficiency.

NASA's Jet Propulsion Laboratory, Pasadena, California

Poly-4-vinylpyridinebisulfate (P4VPBS) is a polymeric salt that has shown promise as a water-free proton-conducting material (solid electrolyte) suitable for use in membrane/electrode assemblies in fuel cells. Heretofore, proton-conducting membranes in fuel cells have been made from perfluorinated ionomers that cannot conduct protons in the absence of water and, consequently, cannot function at temperatures $>100^\circ\text{C}$. In addition, the stability of perfluorinated ionomers at temperatures $>100^\circ\text{C}$ is questionable. However, the performances of fuel cells of the power systems of which they are parts could be improved if operating temperatures could be raised above 140°C . What is needed to make this possible is a solid-electrolyte material, such as P4VPBS, that can be cast into membranes and that both retains proton conductivity and remains stable in the desired higher operating temperature range.

A family of solid-electrolyte materials

different from P4VPBS was described in "Anhydrous Proton-Conducting Membranes for Fuel Cells" (NPO-30493), *NASA Tech Briefs*, Vol. 29, No. 8 (August 2005), page 48. Those materials notably include polymeric quaternized amine salts. If molecules of such a polymeric salt could be endowed with flexible chain structures, it would be possible to overcome the deficiencies of simple organic amine salts that must melt before being able to conduct protons. However, no polymeric quaternized amine salts have yet shown to be useful in this respect.

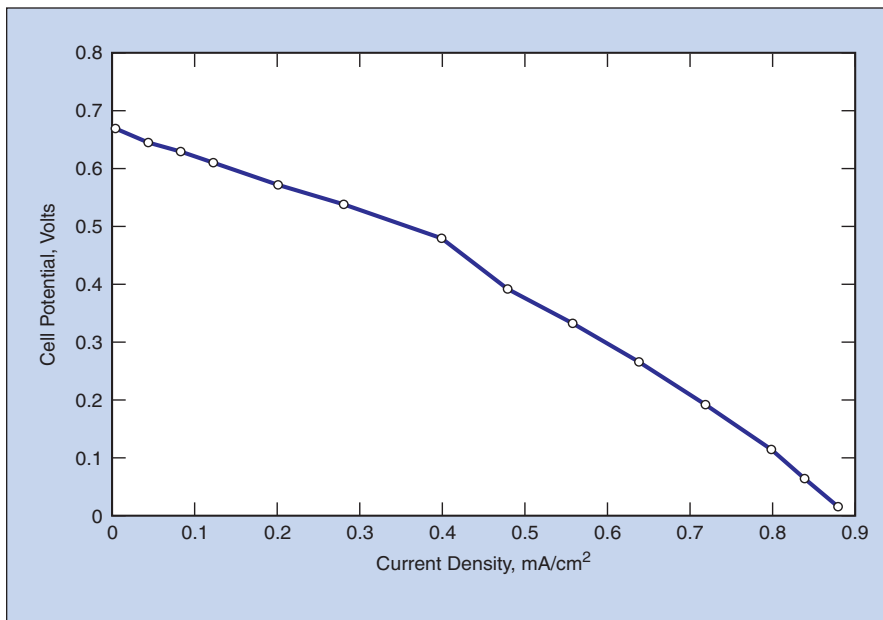
The present solid electrolyte is made by quaternizing the linear polymer poly-4-vinylpyridine (P4VP) to obtain P4VPBS. It is important to start with P4VP having a molecular weight of 160,000 daltons because P4VPBS made from lower-molecular-weight P4VP yields brittle membranes.

In an experimental synthesis, P4VP was dissolved in methanol and then re-

acted with an excess of sulfuric acid to precipitate P4VPBS. The precipitate was recovered, washed several times with methanol to remove traces of acid, and dried to a white granular solid.

In another synthesis, nanoparticles of silica rich with surface hydroxyl groups were added to P4VP in methanol solution, which was then reacted with excess sulfuric acid to precipitate granules of a composite that most probably had the composition $(\text{P4VPBS})\text{-SiO}_2\text{-SiO}(\text{HSO}_4)_2$.

The granular P4VPBS produced in the first-mentioned synthesis was dissolved in water to make a glue-like, turbid solution; the granular P4VPBS/silica composite produced in the second-mentioned synthesis was mixed with water to make a turbid, glue-like suspension. The proportions of polymer salt to water in such preparations can be varied; it was found that approximately equal parts of water and polymer salt yield a solution or suspension amenable to further processing.



Cell Potential vs. Current Density was measured in a test of an experimental membrane/electrode assembly in a hydrogen/oxygen fuel cell at a temperature of 183.5 °C.

Each of these preparations was brushed onto an open mat of glass fibers. The coated mats were dried in flowing air at a temperature of 60 °C for about an hour. The coated mats were further dried in a vacuum oven at 60 °C to remove traces of water.

The thermal stability of P4VPBS was evaluated by differential scanning calorimetry. The results showed that P4VPBS undergoes a glass transition at a temperature of about 182 °C and that it melts at about 298.7 °C, with no evidence of decomposition. These thermal properties are consistent with the requirements for stability under operating conditions in fuel cells.

The coated mats were tested to determine their ionic conductivities and to quantify their performances as membranes in hydrogen/oxygen fuel cells.

The ionic conductivity of the mat coated with the P4VPBS/silica composite was slightly greater than that of the mat coated with P4VPBS: this was expected because the composite contains additional molecular groups that are presumably available for forming hydrogen bonds. On the basis of the observed temperature dependence of the conductivity, the activation energy for conduction was estimated to be about 0.1 eV, suggesting hopping-type conduction through hydrogen bonds. While the measured conductivity values were two orders of magnitude lower than desirable for fuel-cell applications, the degree of solid-state proton conduction was the highest observed thus far in polymeric salts. It is anticipated that the polymer backbone could be modified to facilitate formation of hydrogen bonds to obtain more sites

for proton hopping and, hence, greater proton conductivity.

In preparation for the tests of fuel-cell performance, the coated mats were further coated with catalytic anode and cathode layers to form membrane/electrode assemblies. No attempt was made to optimize the catalytic layers. In the fuel-cell tests, stable maximum cell potentials of 0.85 V were attained. The anticipated maximum cell voltage was 1.0 V. The decrease from the expected maximum value was attributed to some crossover of hydrogen and oxygen through the membranes. The figure shows some of the data from the fuel-cell test of the mat coated with the P4VPBS/silica composite. The power density indicated by these data is low for a fuel cell operating at the indicated temperature — presumably because of the lack of optimization of the catalyst layers. Nevertheless, the data suggest that optimization of catalysts and enhancement of conductivity should make it possible to realize high-temperature fuel cells.

This work was done by Sekharipuram Narayanan and Shiao-Pin Yen of Caltech for NASA's Jet Propulsion Laboratory. Further information is contained in a TSP (see page 1).

In accordance with Public Law 96-517, the contractor has elected to retain title to this invention. Inquiries concerning rights for its commercial use should be addressed to:

*Innovative Technology Assets Management
JPL*

*Mail Stop 202-233
4800 Oak Grove Drive
Pasadena, CA 91109-8099
(818) 354-2240*

E-mail: iaoffice@jpl.nasa.gov

Refer to NPO-30873, volume and number of this NASA Tech Briefs issue, and the page number.



Mo/Ti Diffusion Bonding for Making Thermoelectric Devices

Bonds are mechanically and chemically stable at operating temperatures near 700 °C.

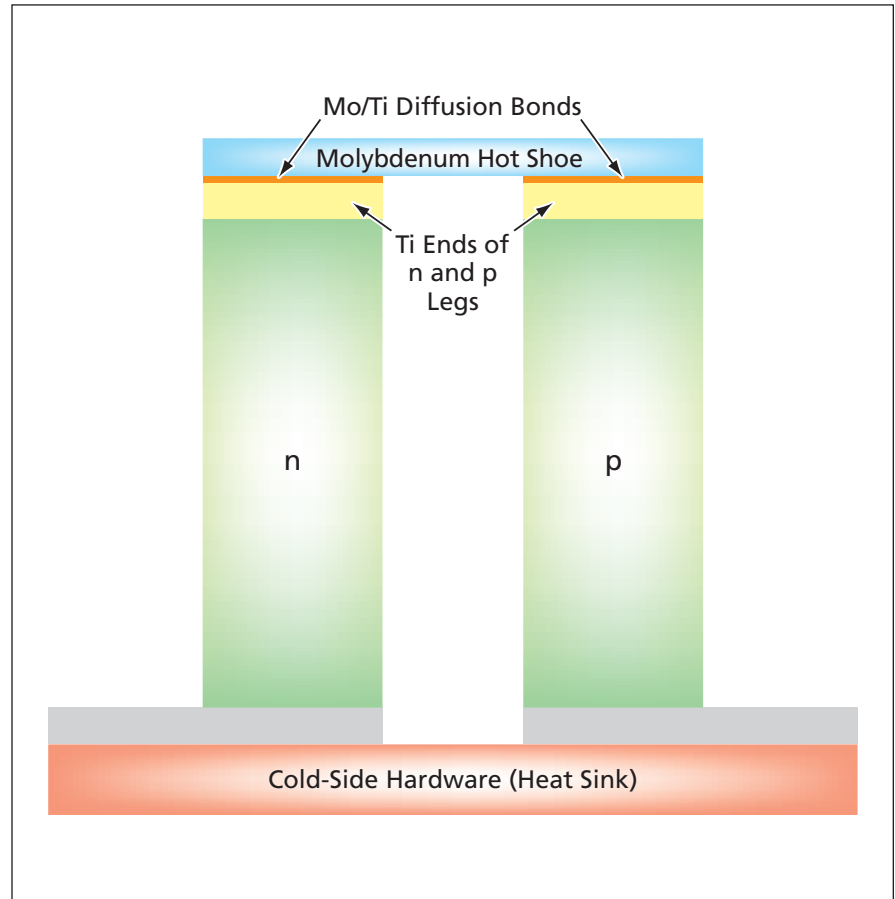
NASA's Jet Propulsion Laboratory, Pasadena, California

An all-solid-state diffusion bonding process that exploits the eutectoid reaction between molybdenum and titanium has been developed for use in fabricating thermoelectric devices based on skutterudite compounds. In essence, the process is one of heating a flat piece of pure titanium in contact with a flat piece of pure molybdenum to a temperature of about 700 °C while pushing the pieces together with a slight pressure [a few psi (of the order of 10 kPa)]. The process exploits the energy of mixing of these two metals to form a strong bond between them. These two metals were selected partly because the bonds formed between them are free of brittle intermetallic phases and are mechanically and chemically stable at high temperatures.

The process is a solution of the problem of bonding hot-side metallic interconnections (denoted “hot shoes” in thermoelectric jargon) to titanium-terminated skutterudite n and p legs during the course of fabrication of a unicouple, which is the basic unit cell of a thermoelectric device (see figure). The hot-side operating temperature required for a skutterudite thermoelectric device is 700 °C. This temperature precludes the use of brazing to attach the hot shoe; because brazing compounds melt at lower temperatures, the hot shoe would become detached during operation. Moreover, the decomposition temperature of one of the skutterudite compounds is 762 °C; this places an upper limit on the temperature used in bonding the hot shoe.

Molybdenum was selected as the interconnection metal because the eutectoid reaction between it and the titanium at the ends of the p and n legs has characteristics that are well suited for this application. In addition to being suitable for use in the present bonding process, molybdenum has high electrical and thermal conductivity and excellent thermal stability — characteristics that are desired for hot shoes of thermoelectric devices.

The process takes advantage of the chemical potential energy of mixing be-



A Molybdenum Hot Shoe is bonded to the titanium tips of the p and n skutterudite legs of a thermoelectric unicouple.

tween molybdenum and titanium. These metals have a strong affinity for each other. They are almost completely soluble in each other and remain in the solid state at temperatures above the eutectoid temperature of 695 °C. As a result, bonds formed by interdiffusion of molybdenum and titanium are mechanically stable at and well above the original bonding temperature of about 700 °C. Inasmuch as the bonds are made at approximately the operating temperature, thermomechanical stresses associated with differences in thermal expansion are minimized.

This work was done by Jeffrey Sakamoto, Adam Kisor, Thierry Caillat, Liana Lara, Vilupanur Ravi, Samad Firdosy, and Jean-

Pierre Fleurial of Caltech for NASA's Jet Propulsion Laboratory. Further information is contained in a TSP (see page 1).

In accordance with Public Law 96-517, the contractor has elected to retain title to this invention. Inquiries concerning rights for its commercial use should be addressed to:

*Innovative Technology Assets Management
JPL*

*Mail Stop 202-233
4800 Oak Grove Drive
Pasadena, CA 91109-8099
(818) 354-2240*

E-mail: iaoffice@jpl.nasa.gov

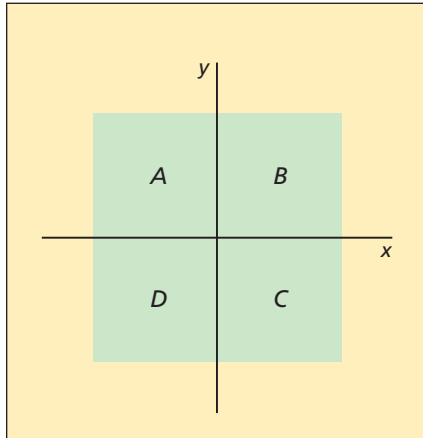
Refer to NPO-40883, volume and number of this NASA Tech Briefs issue, and the page number.

Photodetectors on Coronagraph Mask for Pointing Control

Light from a star under observation would be utilized instead of merely absorbed or suppressed.

NASA's Jet Propulsion Laboratory, Pasadena, California

It has been proposed to install a symmetrical array of photodetectors about the center of the mask of a coronagraph of the type used to search for



A Square or Rectangular Array of four photodetectors would provide indications of the x and y displacements of a star image from the origin, which would lie at the center of a coronagraph mask.

planets orbiting remote stars. The purpose of this installation is to utilize the light from a star under observation as a guide in pointing the telescope. Simple arithmetic processing of the outputs of the photodetectors would provide indications of the lateral position of the center of the mask relative to the center of the image of the star. These indications could serve as pointing-control feedback signals for adjusting the telescope aim to center the image of the star on the mask.

The widths of central mask areas available for placement of photodetectors differ among coronagraph designs, typically ranging upward from about 100 μm . Arrays of photodetectors can readily be placed within areas in this size range. The number of detectors in an array can be as small as 4 or as large as 64. The upper limit on the number of detectors would be determined according to the extent of the occulting pattern and

the number of functionalities, in addition to pointing control, to be served by the array.

In the simplest case, differential position measurements along two orthogonal axes (x and y) could be effected by use of four photodetectors in a square or rectangular array similar to familiar quadrant detectors. Denoting the reading from each photodetector by the letter designation of the photodetector as shown in the figure, the x displacement between the star image and the center of the mask would be proportional to

$$\frac{[(A + D) - (B + C)]}{(A + B + C + D)},$$

while the y displacement would be proportional to

$$\frac{[(A + B) - (C + D)]}{(A + B + C + D)}.$$

This work was done by Kunjithapatham Balasubramanian of Caltech for NASA's Jet Propulsion Laboratory. Further information is contained in a TSP (see page 1). NPO-42552

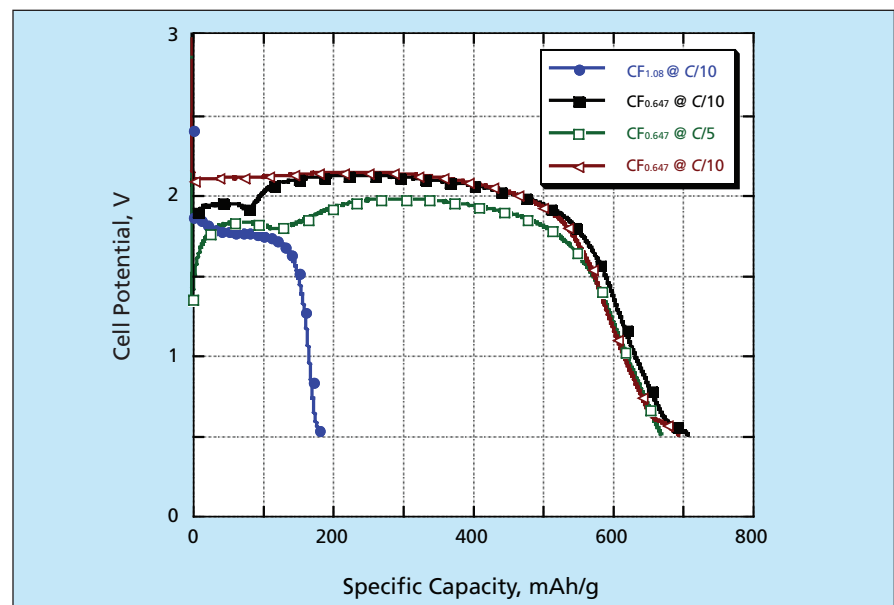
High-Energy-Density, Low-Temperature Li/CF_x Primary Cells

Sub-fluorinated CF_x shows promise as a generic low-temperature cathode material.

NASA's Jet Propulsion Laboratory, Pasadena, California

High-energy-density primary (non-rechargeable) electrochemical cells capable of relatively high discharge currents at temperatures as low as $-40\text{ }^{\circ}\text{C}$ have been developed through modification of the chemistry of commercial Li/CF_x cells and batteries. The commercial Li/CF_x units are not suitable for high-current and low-temperature applications because they are current limited and their maximum discharge rates decrease with decreasing temperature.

The term "Li/CF_x" refers to an anode made of lithium and a cathode made of a fluorinated carbonaceous material (typically graphite). In commercial cells, x typically ranges from 1.05 to 1.1. This cell composition makes it possible to attain specific energies up to 800 Wh/kg, but in order to prevent cell polarization and the consequent large loss of cell capacity, it is typically necessary to keep discharge currents below C/50 (where C is nu-



These Discharge Curves are typical of results of tests, at a temperature of $-40\text{ }^{\circ}\text{C}$, of cells containing fully fluorinated (CF_{1.08}) and sub-fluorinated (CF_{0.65}) cathode materials. These tests were performed at a discharge rate of C/10 and C/5, as labeled. At a potential of 2 V, the CF_{0.65} cathodes exhibited over 3 times the specific capacity of the CF_{1.08} cathode.

merically equal to the current that, flowing during a charge or discharge time of one hour, would integrate to the nominal charge or discharge capacity of a cell). This limitation has been attributed to the low electronic conductivity of CF_x for $x \approx 1$. To some extent, the limitation might be overcome by making cathodes thinner, and some battery manufacturers have obtained promising results using thin cathode structures in spiral configurations.

The present approach includes not only making cathodes relatively thin [≈ 2 mils (≈ 0.051 mm)] but also using sub-fluorinated CF_x cathode materials ($x < 1$) in conjunction with electrolytes formulated for use at low temperatures. The reason for choosing sub-fluorinated CF_x cathode materials is that their electronic conductivities are high, relative to those for which $x > 1$. It was known from recent prior research that cells containing sub-fluorinated CF_x cathodes (x between 0.33 and 0.66) are capable of retaining substantial portions of their nominal low-current specific energies when discharged at rates as high as 5C at room tempera-

ture. However, until experimental cells were fabricated following the present approach and tested, it was not known whether or to what extent low-temperature performance would be improved.

For the experimental cells, cathodes were fabricated by spray deposition of multiple layers of cathode mixtures onto roughened 1-mil (≈ 0.025 -mm)-thick aluminum-foil current collectors. Each cathode mixture consisted of a CF_x powder and carbon black suspended in a binder/solvent solution of poly(vinylidene fluoride) in N-methyl-2-pyrrolidone. For some of the cells, the CF_x was sub-fluorinated by various amounts ($x = 0.53$ or $x = 0.65$). For other cells, used as controls, a fully fluorinated industrial CF_x ($x = 1.08$) was used.

Each resulting cathode structure, 1 to 3 mils (about 0.025 to 0.076 mm) thick, was vacuum furnace dried, then incorporated into a standard coin cell case along with a separator, lithium foil anode, and an electrolyte consisting of $LiBF_4$ dissolved at a concentration of 0.5 M in an 80/20 DME/PC (dimethoxy ethane/propylene carbon-

ate) solvent mixture. The cells were tested in galvanostatic discharges at room temperature and -40 °C at currents from 2C to C/40. The fully fluorinated and sub-fluorinated cells performed comparably at rates as high as 2C at room temperature. At -40 °C, the sub-fluorinated cells exhibited approximately 3 times the specific capacities of the fully fluorinated cells when discharged at C/10 and C/5 discharge rates (see figure).

This work was done by Jay Whitacre, Ratanakumar Bugga, Marshall Smart, G. Prakash, and Rachid Yazami of Caltech for NASA's Jet Propulsion Laboratory. Further information is contained in a TSP (see page 1).

In accordance with Public Law 96-517, the contractor has elected to retain title to this invention. Inquiries concerning rights for its commercial use should be addressed to:

*Innovative Technology Assets Management
JPL*

*Mail Stop 202-2334800 Oak Grove Drive
Pasadena, CA 91109-8099(818) 354-2240
E-mail: iaoffice@jpl.nasa.gov*

Refer to NPO-43219, volume and number of this NASA Tech Briefs issue, and the page number.

G⁴-FETs as Universal and Programmable Logic Gates

Logic functions could be implemented using fewer active circuit elements.

NASA's Jet Propulsion Laboratory, Pasadena, California

An analysis of a patented generic silicon-on-insulator (SOI) electronic device called a G⁴-FET has revealed that the device could be designed to function as a universal and programmable logic gate. The universality and programmability could be exploited to design logic circuits containing fewer discrete components than are required for conventional transistor-based circuits performing the same logic functions.

A G⁴-FET is a combination of a junction field-effect transistor (JFET) and a metal oxide/semiconductor field-effect transistor (MOSFET) superimposed in a single silicon island and can therefore be regarded as two transistors sharing the same body. A G⁴-FET can also be regarded as a single transistor having four gates: two side junction-based gates, a top MOS gate, and a back gate activated by biasing of the SOI substrate. Each of these gates can be used to control the conduction characteristics of the transistor; this possibility creates new options for designing analog,

radio-frequency, mixed-signal, and digital circuitry.

With proper choice of the specific dimensions for the gates, channels, and ancillary features of the generic G⁴-FET, the device could be made to function as a three-input, one-output logic gate. As illustrated by the truth table in the top part of the figure, the behavior of this logic gate would be the inverse (the NOT) of that of a majority gate. In other words, the device would function as a NOT-majority gate. By simply adding an inverter, one could obtain a majority gate. In contrast, to construct a majority gate in conventional complementary metal oxide/semiconductor (CMOS) circuitry, one would need four three-input AND gates and a four-input OR gate, altogether containing 32 transistors.

The middle part of the figure schematically depicts three ways of realizing an inverter (NOT gate), two ways of realizing an AND gate, and two ways of realizing an OR gate by use of one or two NOT-majority gates. In addition

(not shown in the figure), by using one of the three inputs as a programming or control input that is set to 0 or 1, a NOT-majority could be made to respond to the other inputs as either a NAND or a NOR gate, respectively. Inasmuch as the sets {NOT,AND}, {NOT,OR}, and {NAND,NOR} have previously been shown to be universal (in the sense that any digital computation or logic function could be realized by use of suitable combinations of members of these sets), the possibility of realizing these sets signifies that the NOT-majority gate is also universal.

The bottom part of the figure depicts a full adder, implemented by use of three NOT-majority gates and two inverters, that would put out two one-bit binary numbers in response to three input one-bit binary numbers. The design of this adder exploits the possibility of switching a NOT-majority gate between NAND and NOR functionality to minimize the number of gates needed. In contrast, the simplest implementation of

an equivalent full adder based on Boolean gates would include nine NAND gates and four inverters.

This work was done by Travis Johnson, Amir Fijany, Mohammad Mojarradi, Farrokh Vatan, Nikzad Toomarian, Elizabeth Kolawa, Sorin Cristoloveanu, and Benjamin Blalock of Caltech for NASA's Jet Propulsion

Laboratory. Further information is contained in a TSP (see page 1).

In accordance with Public Law 96-517, the contractor has elected to retain title to this invention. Inquiries concerning rights for its commercial use should be addressed to:

*Innovative Technology Assets Management
JPL*

*Mail Stop 202-233
4800 Oak Grove Drive
Pasadena, CA 91109-8099
(818) 354-2240*

*E-mail: iaoffice@jpl.nasa.gov
Refer to NPO-41698, volume and number of this NASA Tech Briefs issue, and the page number.*



Fabrication of Buried Nanochannels From Nanowire Patterns

Sacrificial nanowires are buried, then etched away to form buried channels.

NASA's Jet Propulsion Laboratory, Pasadena, California

A method of fabricating channels having widths of tens of nanometers in silicon substrates and burying the channels under overlying layers of dielectric materials has been demonstrated. With further refinement, the method might be useful for fabricating nanochannels for manipulation and analysis of large biomolecules at single-molecule resolution. Unlike in prior methods, burying the channels does not involve bonding of flat wafers to the silicon substrates to cover exposed channels in the substrates. Instead, the formation and burying of the channels are accomplished in a more sophisticated process that is less vulnerable to defects in the substrates and less likely to result in clogging of, or leakage from, the channels.

In this method, the first step is to establish the channel pattern by forming an array of sacrificial metal nanowires on an SiO₂-on-Si substrate. In particular, the wire pattern is made by use of focused-ion-beam (FIB) lithography and a subsequent metallization/lift-off process. The pattern of metal nanowires is then transferred onto the SiO₂ layer by reactive-ion etching, which yields sacrificial SiO₂ nanowires covered by metal. After re-

moval of the metal covering the SiO₂ nanowires, what remains are SiO₂ nanowires on an Si substrate.

Plasma-enhanced chemical vapor deposition (PECVD) is used to form a layer of a dielectric material over the Si substrate and over the SiO₂ wires on the surface of the substrate. FIB milling is then performed to form trenches at both ends of each SiO₂ wire. The trenches serve as openings for the entry of chem-

icals that etch SiO₂ much faster than they etch Si. Provided that the nanowires are not so long that the diffusion of the etching chemicals is blocked, the sacrificial SiO₂ nanowires become etched out from between the dielectric material and the Si substrate, leaving buried channels. At the time of reporting the information for this article, channels 3 μm long, 20 nm deep, and 80 nm wide (see figure) had been fabricated by this method.

This work was done by Daniel Choi and Eui-Hyeok-Yang of Caltech for NASA's Jet Propulsion Laboratory. Further information is contained in a TSP (see page 1).

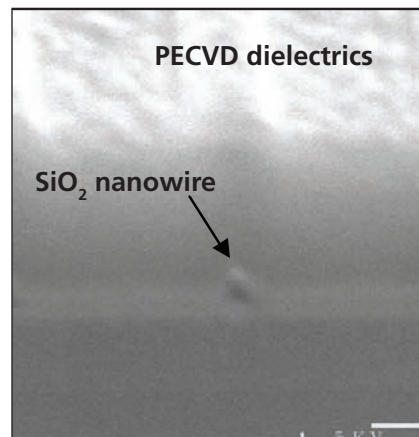
In accordance with Public Law 96-517, the contractor has elected to retain title to this invention. Inquiries concerning rights for its commercial use should be addressed to:

*Innovative Technology Assets Management
JPL*

*Mail Stop 202-233
4800 Oak Grove Drive
Pasadena, CA 91109-8099
(818) 354-2240*

E-mail: iaoffice@jpl.nasa.gov

Refer to NPO-30839, volume and number of this NASA Tech Briefs issue, and the page number.



This Scanning Electron Micrograph shows a cross section of a 20-by-80-nm channel formed between a silicon substrate and an overlying layer of dielectric material.

Diamond Smoothing Tools

Machined surfaces could be made much smoother.

Marshall Space Flight Center, Alabama

Diamond smoothing tools have been proposed for use in conjunction with diamond cutting tools that are used in many finish-machining operations. Diamond machining (including finishing) is often used, for example, in fabrication of precise metal mirrors.

A diamond smoothing tool according to the proposal would have a smooth spherical surface. For a given finish machining operation, the smoothing tool would be mounted next to the cutting

tool. The smoothing tool would slide on the machined surface left behind by the cutting tool, plastically deforming the surface material and thereby reducing the roughness of the surface, closing microcracks and otherwise generally reducing or eliminating microscopic surface and subsurface defects, and increasing the microhardness of the surface layer. It has been estimated that if smoothing tools of this type were used in conjunction with cut-

ting tools on sufficiently precise lathes, it would be possible to reduce the roughness of machined surfaces to as little as 3 nm.

A tool according to the proposal would consist of a smoothing insert in a metal holder. The smoothing insert would be made from a diamond/metal functionally graded composite rod preform, which, in turn, would be made by sintering together a bulk single-crystal or polycrystalline diamond, a diamond

powder, and a metallic alloy at high pressure. To form the spherical smoothing tip, the diamond end of the preform would be subjected to flat grinding, conical grinding, spherical grinding using diamond wheels, and finally spherical polishing and/or buffing using diamond powders. If the dia-

mond were a single crystal, then it would be crystallographically oriented, relative to the machining motion, to minimize its wear and maximize its hardness.

Spherically polished diamonds could also be useful for purposes other than smoothing in finish machining: They

would likely also be suitable for use as heat-resistant, wear-resistant, unlubricated sliding-fit bearing inserts.

This work was done by Oleg Voronov of Diamond Materials, Inc. for Marshall Space Flight Center. Further information is contained in a TSP (see page 1).MFS-32485-1



Infrared Imaging System for Studying Brain Function

This would be an alternative to large, expensive, immobile fMRI systems.

NASA's Jet Propulsion Laboratory, Pasadena, California

A proposed special-purpose infrared imaging system would be a compact, portable, less-expensive alternative to functional magnetic resonance imaging (fMRI) systems heretofore used to study brain function. Whereas a typical fMRI system fills a large room, and must be magnetically isolated, this system would fit into a bicycle helmet.

The system would include an assembly that would be mounted inside the padding in a modified bicycle helmet

or other suitable headgear. The assembly would include newly designed infrared photodetectors and data-acquisition circuits on integrated-circuit chips on low-thermal-conductivity supports in evacuated housings (see figure) arranged in multiple rows and columns that would define image coordinates. Each housing would be spring-loaded against the wearer's head. The chips would be cooled by a small Stirling Engine mounted contiguous to, but ther-

mally isolated from, the portions of the assembly in thermal contact with the wearer's head. Flexible wires or cables for transmitting data from the aforementioned chips would be routed to an integrated, multichannel transmitter and thence through the top of the assembly to a patch antenna on the outside of the helmet.

The multiple streams of data from the infrared-detector chips would be sent to a remote site, where they would be processed, by software, into a three-dimensional display of evoked potentials that would represent firing neuronal bundles and thereby indicate locations of neuronal activity associated with mental or physical activity. The 3D images will be analogous to current fMRI images. The data would also be made available, in real-time, for comparison with data in local or internationally accessible relational databases that already exist in universities and research centers.

Hence, this system could be used in research on, and for the diagnosis of response from the wearer's brain to physiological, psychological, and environmental changes in real time. The images would also be stored in a relational database for comparison with corresponding responses previously observed in other subjects.

This work was done by Frederick Mintz, Philip Moynihan, and Sarath Gunapala of Caltech for NASA's Jet Propulsion Laboratory. Further information is contained in a TSP (see page 1).

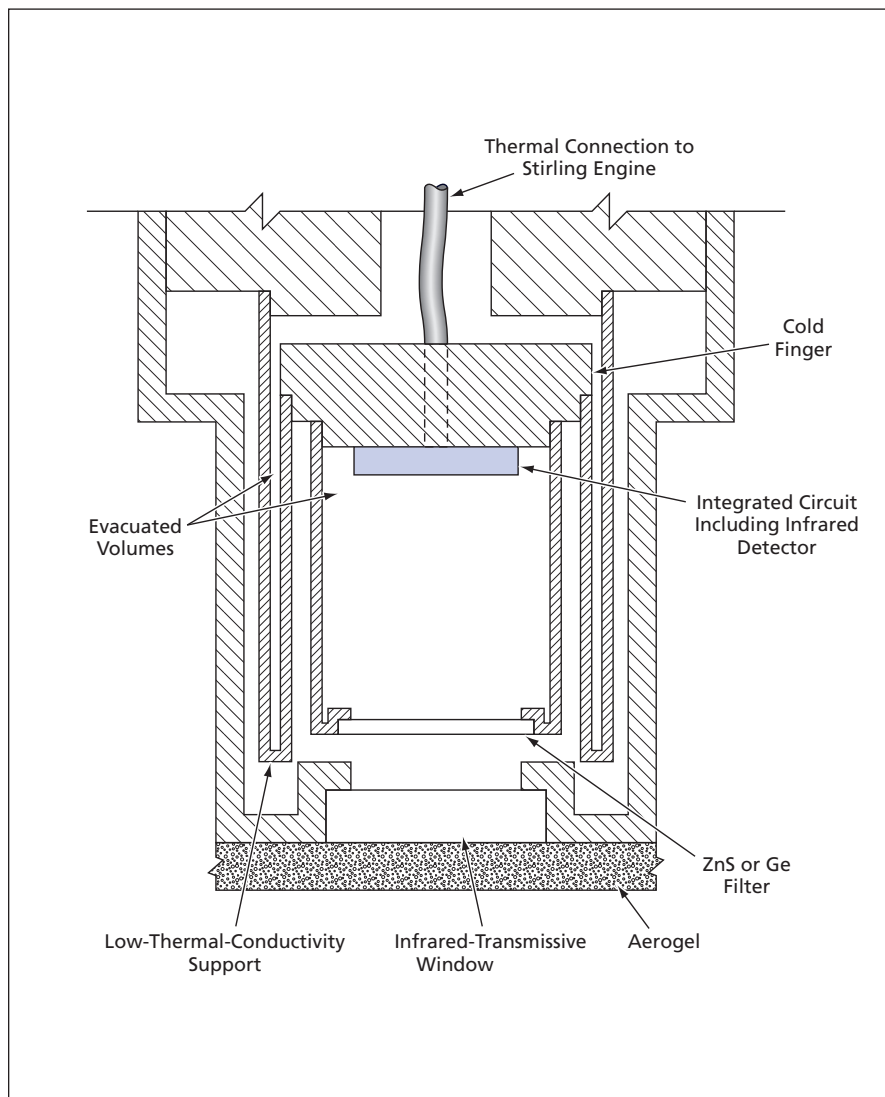
In accordance with Public Law 96-517, the contractor has elected to retain title to this invention. Inquiries concerning rights for its commercial use should be addressed to:

*Innovative Technology Assets Management
JPL*

*Mail Stop 202-233
4800 Oak Grove Drive
Pasadena, CA 91109-8099
(818) 354-2240*

E-mail: iaoffice@jpl.nasa.gov

Refer to NPO-43932, volume and number of this NASA Tech Briefs issue, and the page number.



Each sensor would contain an infrared-detector integrated-circuit chip mounted on a cold finger on a low-thermal-conductivity support in a vacuum.



Rarefying Spectra of Whispering-Gallery-Mode Resonators

Undesired families of resonances are damped by a relatively simple technique.

NASA's Jet Propulsion Laboratory, Pasadena, California

A method of cleaning the mode spectra of whispering-gallery-mode (WGM) optical resonators has been devised to make such resonators more suitable for use as narrow-band optical filters. The method applies, more specifically, to millimeter-sized whispering-gallery-mode optical resonators that are made of crystalline electro-optical materials and have ultrahigh values of the resonance quality factor (Q). The mode spectrum of such a resonator is typically dense, consisting of closely spaced families of modes; as such, the spectrum is not well suited for narrow-band filtering, in which there is a need for strong rejection of side modes. "Cleaning" as used here signifies rarefying the spectrum so that what remains consists mostly of a single desired family of modes or, at worst, a few mode families that are more widely spaced in frequency than are the mode families in the original, non-rarefied spectrum.

The spectrum-cleaning method exploits the fact that various WGM mode families occupy various positions near the equator at the rim of a resonator disk. In this method, a damper in the form of a prism or other polished piece of material having an index of refraction greater than that of the resonator material is placed in contact with the rim of the resonator at such a position that the Q of most or all of the undesired mode families are greatly reduced while the Q of the desired mode family is reduced by only a tolerably small amount. In an alternative method that has been considered, the mode spectrum would be cleaned through special design of the shape of the rim, but fabrication of the rim in a special shape is a complicated task. The advantage of the present method, relative to the alternative method, is that special shaping of the rim is not necessary and the damping prism can be emplaced after the resonator has been fabricated.

This method was demonstrated in an experiment on a WGM resonator in the form of a 12-mm-diameter, 180- μm -thick lithium tantalite disk, the rim of which was polished to a spherical shape. The Q of

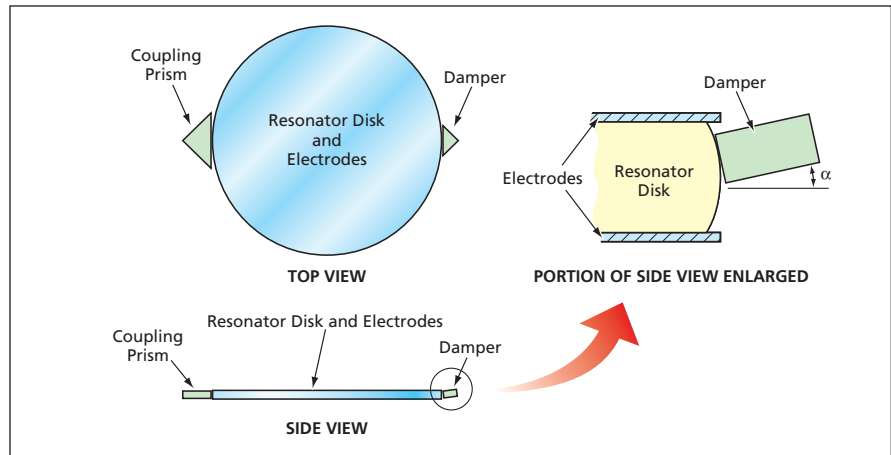


Figure 1. A **WGM Resonator Disk** is equipped with top and bottom tuning electrodes, a coupling prism, and a damper. The placement angle, α , of the damper is adjusted to maximize damping of undesired mode families while not appreciably increasing the damping of desired mode families.

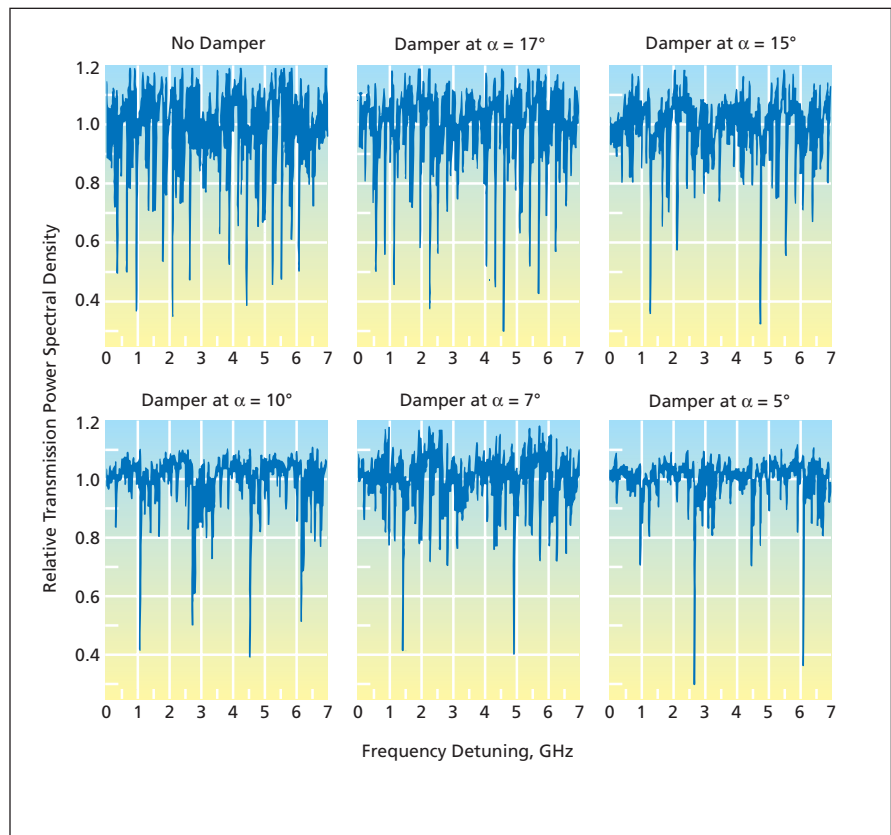


Figure 2. The **Relative-Transmission-Power Spectrum** of a resonator like that of Figure 1 in band-stop configuration was measured without the damper and with the damper placed at various values of α . When the damper was placed at the optimum α , the density of resonant-mode families was significantly reduced.

Large-Area Permanent-Magnet ECR Plasma Source

This device is a good source of ions for plasma processing applications.

John H. Glenn Research Center, Cleveland, Ohio

A 40-cm-diameter plasma device has been developed as a source of ions for material-processing and ion-thruster applications. Like the device described in the immediately preceding article, this device utilizes electron cyclotron resonance (ECR) excited by microwave power in a magnetic field to generate a plasma in an electrodeless (noncontact) manner and without need for an electrically insulating, microwave-transmissive window at the source. Hence, this device offers the same advantages of electrodeless, windowless design — low contamination and long operational life.

The device generates a uniform, high-density plasma capable of sustaining uniform ion-current densities at its exit plane while operating at low pressure [$<10^{-4}$ torr (less than about 1.3×10^{-2} Pa)] and input power <200 W at a frequency of 2.45 GHz. Though the proto-

type model operates at 2.45 GHz, operation at higher frequencies can be achieved by straightforward modification to the input microwave waveguide. Higher frequency operation may be desirable in those applications that require even higher background plasma densities. In the design of this ECR plasma source, there are no cumbersome, power-hungry electromagnets. The magnetic field in this device is generated by a permanent-magnet circuit that is optimized to generate resonance surfaces. The microwave power is injected on the centerline of the device. The resulting discharge plasma jumps into a “high mode” when the input power rises above 150 W. This mode is associated with elevated plasma density and high uniformity.

The large area and uniformity of the plasma and the low operating pressure

are well suited for such material-processing applications as etching and deposition on large silicon wafers. The high exit-plane ion-current density makes it possible to attain a high rate of etching or deposition.

The plasma potential is <3 V — low enough that there is little likelihood of sputtering, which, in plasma processing, is undesired because it is associated with erosion and contamination. The electron temperature is low and does not vary appreciably with power.

This work was done by John E. Foster of Glenn Research Center. Further information is contained in a TSP (see page 1).

Inquiries concerning rights for the commercial use of this invention should be addressed to NASA Glenn Research Center, Commercial Technology Office, Attn: Steve Fedor, Mail Stop 4-8, 21000 Brookpark Road, Cleveland, Ohio 44135. Refer to LEW-17561-1

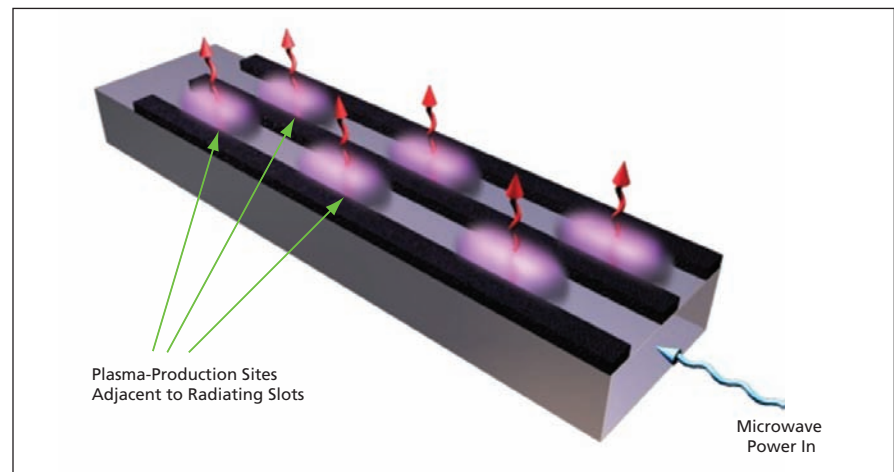
Slot-Antenna/Permanent-Magnet Device for Generating Plasma

Characteristics include uniformity of plasma, scalability, versatility, and long life.

John H. Glenn Research Center, Cleveland, Ohio

A device that includes a rectangular-waveguide/slot-antenna structure and permanent magnets has been devised as a means of generating a substantially uniform plasma over a relatively large area, using relatively low input power and a low gas flow rate. The device utilizes electron cyclotron resonance (ECR) excited by microwave power to efficiently generate plasma in a manner that is completely electrodeless in the sense that, in principle, there is no electrical contact between the plasma and the antenna. Plasmas generated by devices like this one are suitable for use as sources of ions and/or electrons for diverse material-processing applications (e.g., etching or deposition) and for ion thrusters.

The absence of plasma/electrode contact essentially prevents plasma-induced erosion of the antenna, thereby also helping to minimize contamination of the plasma and of objects exposed to the plasma. Consequently, the operational lifetime of the rectangular-waveguide/slot-antenna structure is long and the lifetime of the plasma



Plasma is Produced at sites adjacent to matched radiating slots in a rectangular-waveguide/slot-antenna structure.

source is limited by the lifetime of the associated charged-particle-extraction grid (if used) or the lifetime of the microwave power source.

The device includes a series of matched radiating slot pairs that are distributed along the length of a plasma-

source discharge chamber (see figure). This arrangement enables the production of plasma in a distributed fashion, thereby giving rise to a uniform plasma profile. A uniform plasma profile is necessary for uniformity in any electron- or ion-extraction electrostatic optics. The

slotted configuration of the waveguide/antenna structure makes the device scalable to larger areas and higher powers. All that is needed for scaling up is the attachment of additional matched radiating slots along the length of the discharge chamber. If it is desired to make the power per slot remain constant in scaling up, then the input microwave power must be increased accordingly.

Unlike in prior ECR microwave plasma-generating devices, there is no need for an insulating window on the

antenna. Such windows are sources of contamination and gradually become ineffective as they become coated with erosion products over time. These characteristics relegate prior ECR microwave plasma-generating devices to non-ion beam, non-deposition plasma applications. In contrast, the lack of need for an insulating window in the present device makes it possible to use the device in both ion-beam (including deposition) and electron-beam applications. The device is designed so that ECR takes place

above each slot and the gradient of the magnetic field at each slot is enough to prevent backflow of plasma.

This work was done by John E. Foster of Glenn Research Center. Further information is contained in a TSP (see page 1).

Inquiries concerning rights for the commercial use of this invention should be addressed to NASA Glenn Research Center, Commercial Technology Office, Attn: Steve Fedor, Mail Stop 4-8, 21000 Brookpark Road, Cleveland, Ohio 44135. Refer to LEW-17589-1.

Fiber-Optic Strain Gauge With High Resolution And Update Rate **Changes in strain are correlated with changes in speckle patterns.**

Stennis Space Center, Mississippi

An improved fiber-optic strain gauge is capable of measuring strains in the approximate range of 0 to 50 microstrains with a resolution of 0.1 microstrain. (To some extent, the resolution of the strain gauge can be tailored and may be extensible to 0.01 microstrain.) The total cost of the hardware components of this strain gauge is less than \$100 at 2006 prices. In comparison with prior strain gauges capable of measurement of such low strains, this strain gauge is more accurate, more economical, and more robust, and it operates at a higher update rate. Strain gauges like this one are useful mainly for measuring small strains (including those associated with vibrations) in such structures as rocket test stands, buildings, oilrigs, bridges, and dams. The technology was inspired by the need to measure very small strains on structures supporting liquid oxygen tanks, as a way to measure accurately mass of liquid oxygen during rocket engine testing.

This improved fiber-optic strain gauge was developed to overcome some of the

deficiencies of both traditional foil strain gauges and prior fiber-optic strain gauges. Traditional foil strain gages do not have adequate signal-to-noise ratios at such small strains. Fiber-optic strain gauges have been shown to be potentially useful for measuring such small strains, but heretofore, the use of fiber-optic strain gauges has been inhibited, variously, by complexity, cost, or low update rate.

The improved fiber-optic strain gauge is partially composed of a multi-mode fiber optic which is wound in an elliptical pattern and bonded to the structure of interest. A laser is fixed within an adjustable cylindrical steel enclosure and aimed at one end of the optical fiber. The laser light emerging from the other end of the fiber forms a speckle pattern that changes as strain is applied to the structure. The speckle pattern is intercepted by an array of photocells, so that any change in the speckle pattern manifests itself in changes in the intensities of light measured by the individual photocells. The

outputs of the photocells are collected by a customized data-acquisition system that includes a signal-conditioning subsystem. The photocell outputs are then fed to a neural network that recognizes the correlation between changes in the outputs and changes in strain.

Inasmuch as the changes in the intensities of light incident on the photocells are repeatable for a given amount of change in strain, the neural network can be quickly trained by use of speckle patterns associated with known levels of strain. For measurement of temporally varying strain (for example, when vibrations are present), the update rate and, hence, the dynamic analysis rate depends on the data-acquisition rate.

This work was done by Fernando Figueroa of Stennis Space Center and Ajay Mahajan, Mohammad Sayeh, and Bradley Regez of Southern Illinois University, Carbondale.

Inquiries concerning rights for the commercial use of this invention should be addressed to Intellectual Property Manager, NASA Stennis Space Center; (228) 688-1929. Refer to SSC-00243.

Broadband Achromatic Telecentric Lens

Lens works with a matched spectrometer for applications covering the entire solar-reflected spectrum.

NASA's Jet Propulsion Laboratory, Pasadena, California

A new type of lens design features broadband achromatic performance as well as telecentricity, using a minimum number of spherical elements. With appropriate modifications, the lens design

form can be tailored to cover the range of response of the focal-plane array, from Si (400–1,000 nm) to InGaAs (400–1,700 or 2,100 nm) or InSb/HgCdTe reaching to 2,500 nm. For reference, lenses typically

are achromatized over the visible wavelength range of 480–650 nm.

In remote sensing applications, there is a need for broadband achromatic telescopes, normally satisfied with mirror-

based systems. However, mirror systems are not always feasible due to size or geometry restrictions. They also require expensive aspheric surfaces. Non-observed mirror systems can be difficult to align and have a limited (essentially one-dimensional) field of view. Centrally obscured types have a two-dimensional but very limited field in addition to the obscuration. Telecentricity is a highly desirable property for matching typical spectrometer types, as well as for reducing the variation of the angle of incidence and cross-talk on the detector for simple camera types.

This rotationally symmetric telescope with no obscuration and using spherical surfaces and selected glass types fills a need in the range of short focal lengths. It can be used as a compact front unit for a matched spectrometer, as an ultra-broadband camera objective lens, or as the optics of an integrated camera/spectrometer in which the wavelength information is obtained by the use of strip or linear variable filters on the focal plane array. This kind of camera and spectrometer system can find applications in remote sensing, as well as *in-situ* applications for geologi-

cal mapping and characterization of minerals, ecological studies, and target detection and identification through spectral signatures. Commercially, the lens can be used in quality-control applications via spectral analysis.

The lens design is based on the rear landscape lens with the aperture stop in front of all elements. This allows sufficient room for telecentricity in addition to making the stop easily accessible. The crucial design features are the use of a doublet with an ultra-low dispersion glass (fluorite or SFPL53), and the use of a strong negative element, which enables flat field and telecentricity in conjunction with the last (field lens) element. The field lens also can be designed to be in contact with the array, a feature that is desirable in some applications.

The lens has a 20° field of view, for a 50-mm focal length, and is corrected over the range of wavelengths of 450–2,300 nm. Transverse color, which is the most pernicious aberration for spectroscopic work, is controlled at the level of 1 μm or below at 0.7 μm field and 5 μm at full field. The maximum chief ray angle is less than 1.7°, provid-

ing good telecentricity. An additional feature of this lens is that it is made exclusively with glasses that provide good transmission up to 2,300 nm and even some transmission to 2,500 nm; thus, the lens can be used in applications that cover the entire solar-reflected spectrum. Alternative realizations are possible that provide enhanced resolution and even less transverse color over a narrower wavelength range.

This work was done by Pantazis Mouroulis of Caltech for NASA's Jet Propulsion Laboratory. Further information is contained in a TSP (see page 1).

In accordance with Public Law 96-517, the contractor has elected to retain title to this invention. Inquiries concerning rights for its commercial use should be addressed to:

*Innovative Technology Assets Management
JPL*

*Mail Stop 202-233
4800 Oak Grove Drive
Pasadena, CA 91109-8099
(818) 354-2240*

E-mail: iaoffice@jpl.nasa.gov

Refer to NPO-44059, volume and number of this NASA Tech Briefs issue, and the page number.



Temperature-Corrected Model of Turbulence in Hot Jet Flows

A standard turbulence model is corrected for total-temperature gradient and compressibility.

Langley Research Center, Hampton, Virginia

An improved correction has been developed to increase the accuracy with which certain formulations of computational fluid dynamics predict mixing in shear layers of hot jet flows. The CFD formulations in question are those derived from the Reynolds-averaged Navier-Stokes equations closed by means of a two-equation model of turbulence, known as the $k-\epsilon$ model, wherein effects of turbulence are summarized by means of an eddy viscosity. The need for a correction arises because it is well known among specialists in CFD that two-equation turbulence models, which were developed and calibrated for room-temperature, low Mach-number, plane-mixing-layer flows, underpredict mixing in shear layers of hot jet flows. The present correction represents an attempt to account for increased mixing that takes place in jet flows characterized

by high gradients of total temperature. This correction also incorporates a commonly accepted, previously developed correction for the effect of compressibility on mixing.

One of the two equations of the $k-\epsilon$ model is

$$\mu_t = \rho C_\mu k^2/\epsilon,$$

where μ_t is the eddy viscosity, ρ is the mass density, k is the time-averaged kinetic-energy density associated with the local fluctuating (turbulent) component of flow, ϵ is the time-averaged rate of dissipation of the turbulent-kinetic-energy density, and C_μ is the subject of the present correction, as described next.

In the uncorrected $k-\epsilon$ model, C_μ has the constant value of 0.09. The present correction alters the value of C_μ to approximate the effects of the temperature

gradient and compressibility on the eddy viscosity. Before presenting the correction, it is necessary to define some algebraic terms:

- The temperature correction enters through a function of the gradient of the total temperature normalized by the local turbulence length scale. This function is given by

$$T_g \equiv |\nabla T_t| k^{3/2}/\epsilon T_t,$$

where T_t is the total temperature.

- The turbulence Mach number is given by

$$M_\tau \equiv (2k)^{1/2}/a,$$

where a is the local speed of sound.

- The compressibility correction enters through a function of the turbulence Mach number. This function is given by

$$f(M_\tau) = (M_\tau^2 - M_{\tau 0}^2)H(M_\tau - M_{\tau 0}),$$

where $H(x)$ is the Heaviside function of x (the unit step function of x , which is 0 for negative x and 1 for positive x), and $M_{\tau 0}$ is a threshold M_τ value (initially set at 0.1) below which it is deemed unnecessary to apply the compressibility correction.

Then the corrected value of C_μ is given by

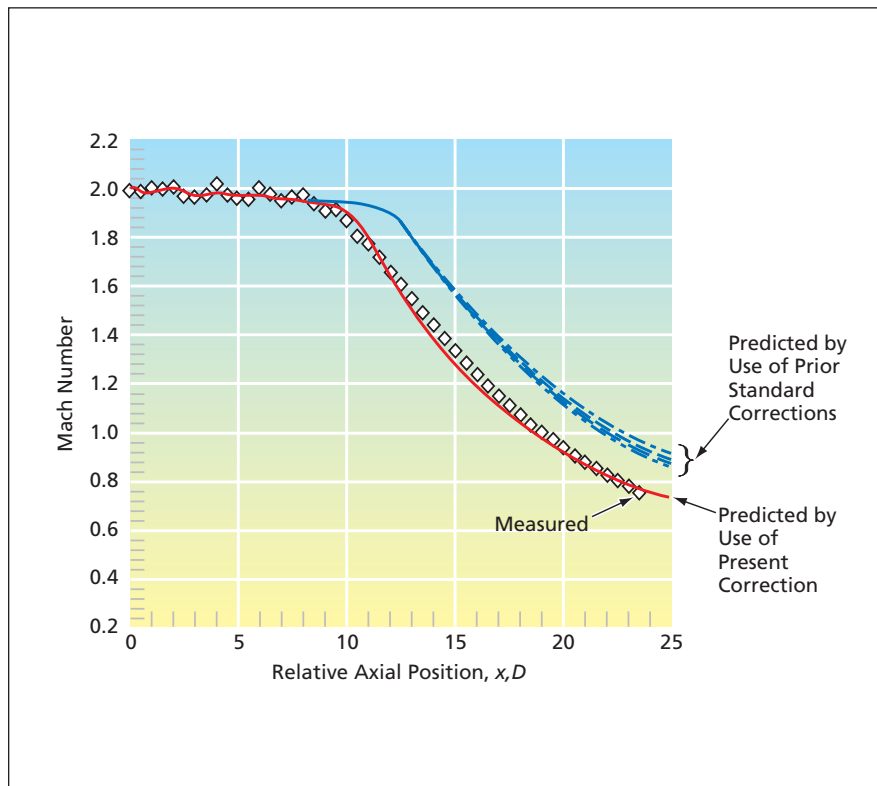
$$C_\mu = 0.09 \left[1 + \frac{T_g^3}{0.041 + f(M_\tau)} \right]$$

It should be noted that in the case of zero total-temperature gradient, the corrected value of C_μ reverts to the prior constant value of 0.09.

The present correction was tested on experimental data, in comparison with four prior standard corrections to the $k-\epsilon$ model. The figure presents an example showing that predictions by use of the present correction were in closest agreement with the experimental data.

This work was done by Khaled S. Abdol-Hamid and S. Paul Pao of Langley Research Center; Steven J. Massey of Eagle Aeronautics, Inc.; and Alaa Elmiligui of Analytical Services & Materials, Inc. Further information is contained in a TSP (see page 1).

LAR-17016-1



The Center-Line Mach Number of a supersonic jet from an axisymmetric nozzle with a plenum total temperature of 2,009 R (=1,116 K) and an exit diameter (D) of 3.60 in. (9.144 cm) was measured and calculated as a function of axial position (x).

Enhanced Elliptic Grid Generation

Decay parameters that govern grids near boundaries are determined automatically.

Ames Research Center, Moffett Field, California

An enhanced method of elliptic grid generation has been invented. Whereas prior methods require user input of certain grid parameters, this method provides for these parameters to be determined automatically.

“Elliptic grid generation” signifies generation of generalized curvilinear coordinate grids through solution of elliptic partial differential equations (PDEs). Usually, such grids are fitted to bounding bodies and used in numerical solution of other PDEs like those of fluid flow, heat flow, and electromagnetics. Such a grid is smooth and has continuous first and second derivatives (and possibly also continuous higher-order derivatives), grid lines are appropriately stretched or clustered, and grid lines are orthogonal or nearly so over most of the grid domain. The source terms in the grid-generating PDEs (hereafter called “defining” PDEs) make it possible for the grid to satisfy requirements for clustering and orthogonality properties in the vicinity of specific surfaces in three dimensions or in the vicinity of specific lines in two dimensions.

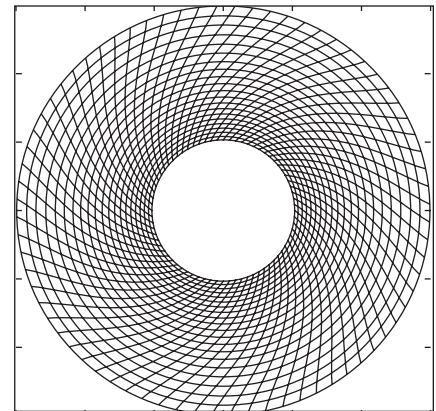
The grid parameters in question are decay parameters that appear in the source terms of the inhomogeneous defining PDEs. The decay parameters are characteristic lengths in exponential-decay factors that express how the influences of the boundaries decrease with distance from the boundaries. These terms govern the rates at which distance between adjacent grid lines change with distance from nearby boundaries.

Heretofore, users have arbitrarily specified decay parameters. However, the characteristic lengths are coupled with the strengths of the source terms, such that arbitrary specification could

lead to conflicts among parameter values. Moreover, the manual insertion of decay parameters is cumbersome for static grids and infeasible for dynamically changing grids.

In the present method, manual insertion and user specification of decay parameters are neither required nor allowed. Instead, the decay parameters are determined automatically as part of the solution of the defining PDEs. Depending on the shape of the boundary segments and the physical nature of the problem to be solved on the grid, the solution of the defining PDEs may provide for rates of decay to vary along and among the boundary segments and may lend itself to interpretation in terms of one or more physical quantities associated with the problem.

The limiting form of the defining equations used in this method is partly analogous to boundary-value PDEs for heat transfer over long, thin fins governing convection and conduction of heat across the boundary segments and heat generated or lost within the volume to be enclosed by the grid. Each limiting form of the defining equations is deemed to be valid near at least one boundary segment. Each such equation includes at least two independent Cartesian coordinate variables and at least one generalized coordinate as a dependent variable, the integral form of which constitutes a boundary constraint. Boundary conditions analogous to temperature and thermal conductivity prescription can be specified by the user. In addition, as an essential element of the method, a selected power of at least one heat-transfer coefficient must correspond to at least one decay parameter (which, as stated above, the user does



A Grid in an Annulus between relatively rotating inner and outer circles was generated by the present method.

not specify) near at least one boundary segment, and such a heat-transfer coefficient evolves according to the boundary constraint.

The figure presents results of application of the method to a two-dimensional annular region. This example illustrates the clustering of grid points near the inner boundary of the annulus. It also illustrates how the grid evolves automatically with one or more time-varying boundary condition(s) — in this case, rotation of the inner boundary relative to the outer boundary or vice versa. In a case involving time-varying boundary conditions, the solution at each time step serves as a starting point for the solution at the next time step.

This work was done by Upender K. Kaul of Ames Research Center.

Inquiries concerning rights for the commercial use of this invention should be addressed to the Technology Partnerships Division, Ames Research Center, (650) 604-2954. Refer to ARC-14710-1

Automated Knowledge Discovery From Simulators

Active learning process efficiently explores simulator input space.

NASA's Jet Propulsion Laboratory, Pasadena, California

A computational method, SimLearn, has been devised to facilitate efficient knowledge discovery from simulators. Simulators are complex computer programs used in science and engineering to model diverse phenomena such as fluid

flow, gravitational interactions, coupled mechanical systems, and nuclear, chemical, and biological processes. SimLearn uses active-learning techniques to efficiently address the “landscape characterization problem.” In particular, SimLearn

tries to determine which regions in “input space” lead to a given output from the simulator, where “input space” refers to an abstraction of all the variables going into the simulator, e.g., initial conditions, parameters, and interaction equations.

Landscape characterization can be viewed as an attempt to invert the forward mapping of the simulator and recover the inputs that produce a particular output.

Given that a single simulation run can take days or weeks to complete even on a large computing cluster, SimLearn attempts to reduce costs by reducing the number of simulations needed to effect discoveries. Unlike conventional data-mining methods that are applied to static predefined datasets, SimLearn involves an iterative process in which a “most informative” dataset is constructed dynamically by using the simulator as an oracle. On each iteration, the algorithm models the knowledge it has gained through previous simulation trials and then chooses which simulation trials to run next. Running these trials through the simulator produces new data in the form of input-output pairs.

The overall process is embodied in an algorithm that combines support vector machines (SVMs) with active learning. SVMs use learning from examples (the examples are the input-output pairs generated by running the simulator) and a principle called maximum margin to derive predictors that generalize well to new inputs. In SimLearn, the SVM plays the

role of modeling the knowledge that has been gained through previous simulation trials. Active learning is used to determine which new input points would be most informative if their output were known. The selected input points are run through the simulator to generate new information that can be used to refine the SVM. The process is then repeated. SimLearn carefully balances exploration (semi-randomly searching around the input space) versus exploitation (using the current state of knowledge to conduct a tightly focused search).

During each iteration, SimLearn uses not one, but an ensemble of SVMs. Each SVM in the ensemble is characterized by different hyperparameters that control various aspects of the learned predictor — for example, whether the predictor is constrained to be very smooth (nearby points in input space lead to similar output predictions) or whether the predictor is allowed to be “bumpy.” The various SVMs will have different preferences about which input points they would like to run through the simulator next. SimLearn includes a formal mechanism for balancing the ensemble SVM preferences so that a single choice can be made for the next set of trials.

Initial tests with two real-world scien-

tific simulators have shown that SimLearn is effective in reducing the number of trials needed to accurately identify the regions of input space leading to particular output behaviors. In the first application involving simulations of collisions between asteroids and the gravitational interactions between the resulting fragments, parameters of the two colliding asteroids that lead to binary pairs (gravitationally bound fragments in orbit around a common center of mass) were identified using only half the simulation trials needed to obtain equivalent knowledge from a grid-based sampling approach. In the second application involving simulations of the Earth’s magnetosphere, there was a corresponding reduction by a factor of six in the number of simulation trials required.

This work was performed by Michael Burl, Dennis DeCoste, Dominic Mazzoni, and Lucas Scharenbroich of Caltech and Brian Enke and William Mertine of the Southwest Research Institute for NASA’s Jet Propulsion Laboratory. Further information is contained in a TSP (see page 1).

The software used in this innovation is available for commercial licensing. Please contact Karina Edmonds of the California Institute of Technology at (626) 395-2322. Refer to NPO-43399.

Σ Electro-Optical Modulator Bias Control Using Bipolar Pulses

Bias is automatically adjusted to maintain maximum extinction during “off” periods.

NASA’s Jet Propulsion Laboratory, Pasadena, California

An improved method has been devised for controlling the DC bias applied to an electro-optical crystal that is part of a Mach-Zehnder modulator that generates low-duty-cycle optical pulses for a pulse-position modulation (PPM) optical data-communication system. In such a system, it is desirable to minimize the transmission of light during the intervals between pulses, and for this purpose, it is necessary to maximize the extinction ratio of the modulator (the ratio between the power transmitted during an “on” period and the power transmitted during an “off” period). The present method is related to prior dither error feedback methods, but unlike in those methods, there is no need for an auxiliary modulation subsystem to generate a dithering signal. Instead, as described below, dither is effected through alternation of the polarity of the modulation signal.

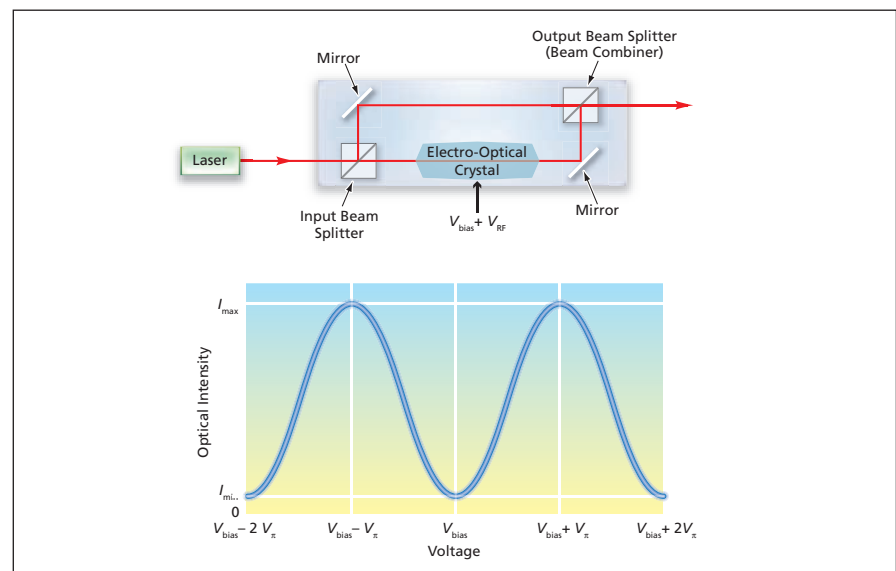


Figure 1. A **Mach-Zehnder Modulator** is a Mach-Zehnder interferometer that includes an electro-optical crystal for varying the difference between the lengths of its two optical paths. If V_{bias} is set at the optimum value, then the output optical power varies as a symmetrical function of V_{RF} .

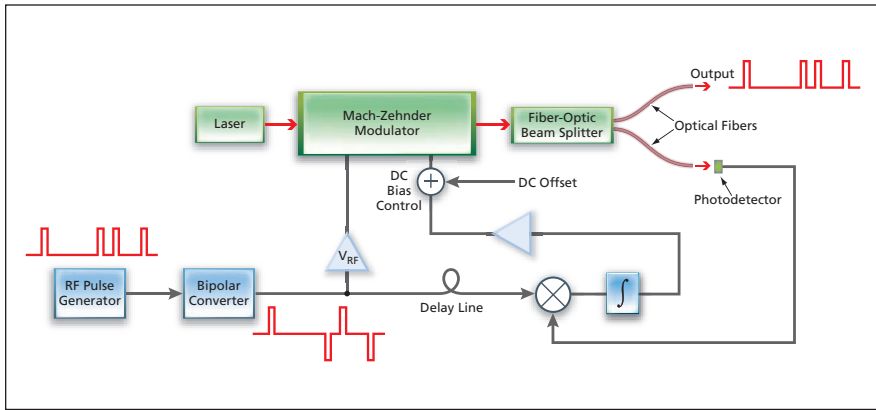


Figure 2. This **Modulation System** for PPM optical communication includes a bias control loop that corrects for electrical and thermal drifts to maintain a maximum extinction ratio.

The upper part of Figure 1 schematically depicts a Mach-Zehnder modulator. The signal applied to the electro-optical crystal consists of a radio-frequency modulating pulse signal, V_{RF} , superimposed on a DC bias V_{bias} . Maximum extinction occurs during the “off” ($V_{RF} = 0$) period if V_{bias} is set at a value that makes the two optical paths differ by an odd integer multiple of a half wavelength so that the beams traveling along the two paths interfere destructively at the output beam splitter. Assuming that the modulating pulse signal V_{RF} has a rectangular waveform, maximum transmission occurs during the “on” period if the amplitude of V_{RF} is set to a value, V_p , that shifts the length

of the affected optical path by a half wavelength so that now the two beams interfere constructively at the output beam splitter.

The modulating pulse signal is AC-coupled from an amplifier to the electro-optical crystal. Sometimes, two successive pulses occur so close in time that the operating point of the amplifier drifts, one result being that there is not enough time for the signal level to return to ground between pulses. Also, the difference between the optical-path lengths can drift with changes in temperature and other spurious effects. The effects of both types of drift are suppressed in the present method, in which one takes advantage of

the fact that when V_{bias} is set at the value for maximum extinction, equal-magnitude positive and negative pulses applied to the electro-optical crystal produce equal output light pulses.

In a modulation system designed and operated according to this method (see Figure 2), the modulating pulses are converted to alternating polarity, a small portion of optical output power is sampled by a photodetector, the photodetector output is multiplied by a sample of the alternating-polarity modulating signal, and the product is integrated over time to obtain an error signal. When V_{bias} is not at the optimum, maximum-extinction value, there is either an overshoot or an undershoot in the output light pulse, such that the integral signal amounts to an error signal that is proportional, in both magnitude and sign, to the difference between the actual and optimum values of V_{bias} . The integral signal is amplified and added to a DC offset voltage, and the sum fed to a bias control input terminal to drive the modulator toward optimum bias. Normally, the DC offset voltage would be set initially at a maximum-extinction point.

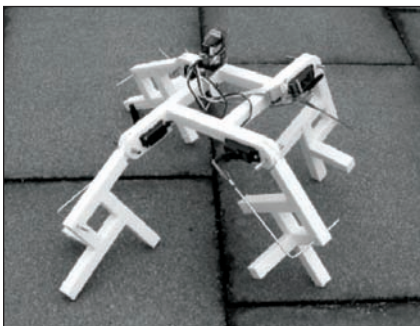
This work was done by William Farr and Joseph Kovalik of Caltech for NASA's Jet Propulsion Laboratory. Further information is contained in a TSP (see page 1). NPO-41301

Generative Representations for Automated Design of Robots

Compact representations circumvent the computational obstacle to complexity.

Ames Research Center, Moffett Field, California

A method of automated design of complex, modular robots involves an evolutionary process in which generative representations of designs are used. The term “generative representations” as used here signifies, loosely, representations that consist of or include algo-



The “Quatrobot” is a Walking Robot that was designed by automated evolutionary synthesis, using a generative representation. The robot was built after 13 iterations.

rithms, computer programs, and the like, wherein encoded designs can reuse elements of their encoding and thereby evolve toward greater complexity.

Automated design of robots through synthetic evolutionary processes has already been demonstrated, but it is not clear whether genetically inspired search algorithms can yield designs that are sufficiently complex for practical engineering. The ultimate success of such algorithms as tools for automation of design depends on the scaling properties of representations of designs. A non-generative representation (one in which each element of the encoded design is used at most once in translating to the design) scales linearly with the number of elements. Search algorithms that use non-generative representations quickly become intractable (search times vary approximately exponentially with numbers of de-

sign elements), and thus are not amenable to scaling to complex designs.

Generative representations are compact representations and were devised as means to circumvent the above-mentioned fundamental restriction on scalability. In the present method, a robot is defined by a compact programmatic form (its generative representation) and the evolutionary variation takes place on this form. The evolutionary process is an iterative one, wherein each cycle consists of the following steps:

1. Generative representations are generated in an evolutionary subprocess.
2. Each generative representation is a program that, when compiled, produces an assembly procedure.
3. In a computational simulation, a constructor executes an assembly procedure to generate a robot.
4. A physical-simulation program tests

the performance of a simulated constructed robot, evaluating the performance according to a fitness criterion to yield a figure of merit that is fed back into the evolutionary subprocess of the next iteration.

In comparison with prior approaches to automated evolutionary design of robots, the use of generative representations offers two advantages: First, a generative representation enables the reuse of components in regular and hierarchical ways and thereby serves a systematic means of creating more complex modules out of

simpler ones. Second, the evolved generative representation may capture intrinsic properties of the design problem, so that variations in the representations move through the design space more effectively than do equivalent variations in a non-generative representation.

This method has been demonstrated by using it to design some robots that move, variously, by walking, rolling, or sliding. Some of the robots were built (see figure). Although these robots are very simple, in comparison with robots designed by humans, their structures are more reg-

ular, modular, hierarchical, and complex than are those of evolved designs of comparable functionality synthesized by use of nongenerative representations.

This work was done by Gregory S. Hornby of Ames Research Center, Hod Lipson of Cornell University, and Jordan B. Pollack of Brandeis University. Further information is contained in a TSP (see page 1).

Inquiries concerning rights for the commercial use of this invention should be addressed to the Technology Partnerships Division, Ames Research Center, (650) 604-2954. Refer to ARC-15334-1



Books & Reports

Mars-Approach Navigation Using *In Situ* Orbiters

A document discusses the continuing development of a navigation system that would enable a spacecraft to approach Mars on a trajectory precise enough to enable the spacecraft to land within 1 km of a specified location on the Martian surface. This degree of accuracy would represent an order-of-magnitude improvement over that now obtained in radiometric tracking by use of the Deep Space Network. The navigation system would be implemented largely in software running in digital processors in the Electra transceiver, the Mars Network's standard radio transceiver, that would be in both the approaching spacecraft and Mars Network orbiter. The Mars Network is an *ad hoc* constellation of existing and future Mars science orbiters and dedicated telecommunication orbiters that has been established as a communication and navigation infrastructure to support the exploration of Mars. The software would exploit the sensory and data-processing capabilities of the Electra transceivers to gather Doppler-shift and other radiometric tracking data and process those data into trajectories data that would be accurate to within 0.3 km at the point of entry into the Martian atmosphere (as needed to land within 1 km of a target surface location).

This work was done by Courtney Duncan and Todd Ely of Caltech and E. Glenn Lightsey of the University of Texas at Austin for NASA's Jet Propulsion Laboratory. Further information is contained in a TSP (see page 1).

The software used in this innovation is available for commercial licensing. Please contact Karina Edmonds of the California Institute of Technology at (626) 395-2322. Refer to NPO-43092.

Efficient Optimization of Low-Thrust Spacecraft Trajectories

A paper describes a computationally efficient method of optimizing trajectories of spacecraft driven by propulsion systems that generate low thrusts and, hence, must be operated for long times. A common goal in trajectory-optimization problems is to find minimum-time, minimum-fuel, or Pareto-optimal trajectories (here, Pareto-optimality signifies

that no other solutions are superior with respect to both flight time and fuel consumption). The present method utilizes genetic and simulated-annealing algorithms to search for globally Pareto-optimal solutions. These algorithms are implemented in parallel form to reduce computation time. These algorithms are coupled with either of two traditional trajectory-design approaches called "direct" and "indirect." In the direct approach, thrust control is discretized in either arc time or arc length, and the resulting discrete thrust vectors are optimized. The indirect approach involves the primer-vector theory (introduced in 1963), in which the thrust control problem is transformed into a co-state control problem and the initial values of the co-state vector are optimized. In application to two example orbit-transfer problems, this method was found to generate solutions comparable to those of other state-of-the-art trajectory-optimization methods while requiring much less computation time.

This work was done by Seungwon Lee, Wolfgang Fink, Ryan Russell, Richard Terrile, Anastassios Petropoulos, and Paul von Allmen of Caltech for NASA's Jet Propulsion Laboratory. Further information is contained in a TSP (see page 1).

The software used in this innovation is available for commercial licensing. Please contact Karina Edmonds of the California Institute of Technology at (626) 395-2322. Refer to NPO-42975.

Cylindrical Asymmetrical Capacitors for Use in Outer Space

A report proposes that cylindrical asymmetrical capacitors (CACs) be used to generate small thrusts for precise maneuvering of spacecraft on long missions. The report notes that it has been known for decades that when high voltages are applied to CACs in air, thrusts are generated — most likely as a result of ionization of air molecules and acceleration of the ions by the high electric fields. The report goes on to discuss how to optimize the designs of CACs for operation as thrusters in outer space. Components that could be used to enable outer-space operation include a supply of gas and a shroud, partly surrounding a CAC, into which the gas would flow. Other elements of operation and design discussed

in the report include variation of applied voltage and/or of gas flow to vary thrust, effects of CAC and shroud dimensions on thrust and weight, some representative electrode configurations, and several alternative designs, including one in which the basic CAC configuration would be modified into something shaped like a conventional rocket engine with converging/diverging nozzle and an anode with gas feed in the space that, in a conventional rocket engine, would be the combustion chamber.

This work was done by Jonathan W. Campbell of Marshall Space Flight Center. Further information is contained in a TSP (see page 1).

This invention has been patented by NASA (U.S. Patent No. 6,775,123). Inquiries concerning nonexclusive or exclusive license for its commercial development should be addressed to Sammy Nabors, MSFC Commercialization Assistance Lead, at sammy.a.nabors@nasa.gov. Refer to MFS-31887-1.

Protecting Against Faults in JPL Spacecraft

A paper discusses techniques for protecting against faults in spacecraft designed and operated by NASA's Jet Propulsion Laboratory (JPL). The paper addresses, more specifically, fault-protection requirements and techniques common to most JPL spacecraft (in contradistinction to unique, mission specific techniques), standard practices in the implementation of these techniques, and fault-protection software architectures. Common requirements include those to protect onboard command, data-processing, and control computers; protect against loss of Earth/spacecraft radio communication; maintain safe temperatures; and recover from power overloads. The paper describes fault-protection techniques as part of a fault-management strategy that also includes functional redundancy, redundant hardware, and autonomous monitoring of (1) the operational and "health" statuses of spacecraft components, (2) temperatures inside and outside the spacecraft, and (3) allocation of power. The strategy also provides for preprogrammed automated responses to anomalous conditions. In addition, the software running in almost every

JPL spacecraft incorporates a general-purpose “Safe Mode” response algorithm that configures the spacecraft in a lower-power state that is safe and predictable, thereby facilitating diagnosis of more complex faults by a team of human experts on Earth.

This work was done by Paula Morgan of Caltech for NASA’s Jet Propulsion Laboratory. Further information is contained in a TSP (see page 1).

The software used in this innovation is available for commercial licensing. Please contact Karina Edmonds of the California Institute of Technology at (626) 395-2322. Refer to NPO-42900.

Algorithm Optimally Allocates Actuation of a Spacecraft

A report presents an algorithm that solves the following problem: Allocate the force and/or torque to be exerted by each thruster and reaction-wheel assembly on a spacecraft for best performance, defined as minimizing the error between (1) the total force and torque commanded by the spacecraft control system and (2) the total of forces and torques actually exerted by all the thrusters and reaction wheels. The algorithm incorporates the matrix-vector relationship between (1) the total applied force and torque and (2) the individual actuator force and torque values. It takes account of such constraints as lower and upper limits on the force or torque that can be applied by a given actuator. The algorithm divides the aforementioned problem into two optimization problems that it solves sequentially. These problems are of a type, known in the art as semi-definite programming problems, that involve linear matrix inequalities. The algorithm incorporates, as subalgorithms, prior algorithms that solve such optimization problems very efficiently. The algorithm

affords the additional advantage that the solution requires the minimum rate of consumption of fuel for the given best performance.

This work was done by Behçet Açıkmese and Shui Motaghedi of Caltech for NASA’s Jet Propulsion Laboratory. Further information is contained in a TSP (see page 1).

The software used in this innovation is available for commercial licensing. Please contact Karina Edmonds of the California Institute of Technology at (626) 395-2322. Refer to NPO-42301.

Radar Interferometer for Topographic Mapping of Glaciers and Ice Sheets

A report discusses Ka-band (35-GHz) radar for mapping the surface topography of glaciers and ice sheets at high spatial resolution and high vertical accuracy, independent of cloud cover, with a swath-width of 70 km. The system is a single-pass, single-platform interferometric synthetic aperture radar (InSAR) with an 8-mm wavelength, which minimizes snow penetration while remaining relatively impervious to atmospheric attenuation.

As exhibited by the lower frequency SRTM (Shuttle Radar Topography Mission) AirSAR and GeoSAR systems, an InSAR measures topography using two antennas separated by a baseline in the cross-track direction, to view the same region on the ground. The interferometric combination of data received allows the system to resolve the path-length difference from the illuminated area to the antennas to a fraction of a wavelength. From the interferometric phase, the height of the target area can be estimated. This means an InSAR system is capable of providing not only the position of each image point in along-track and slant range as with a traditional SAR but also the height of that point through interferometry.

Although the evolution of InSAR to a millimeter-wave center frequency maximizes the interferometric accuracy from a given baseline length, the high frequency also creates a fundamental problem of swath coverage versus signal-to-noise ratio. While the length of SAR antennas is typically fixed by mass and stowage or deployment constraints, the width is constrained by the desired illuminated swath width which sets the swath size is proportional to the wavelength, a fixed swath size equates to a smaller antenna as the frequency is increased. This loss of antenna size reduces the two-way antenna gain to the second power, drastically reducing the signal-to-noise ratio of the SAR system. This fundamental constraint of high-frequency SAR systems is addressed by applying digital beam-forming (DBF) techniques to synthesize multiple simultaneous receive beams in elevation while maintaining a broad transmit illumination. Through this technique, a high antenna gain on receive is preserved, thereby reducing the required transmit power and thus enabling high-frequency SARs and high-precision InSAR from a single spacecraft.

The Ka-band digital beam-forming interferometric mapper will provide critical data on the mass changes of the Earth’s ice cover and contribute data to improved estimates of ice sheet contribution to sea-level rise, as outlined in the Climate Variability and Change road map. The comprehensive measurements will come from the swath, temporal sampling capability, variable resolution, and accuracies unique to this system.

This work was done by Delwyn K. Moller, Gregory A. Sadowy, Eric J. Rignot, and Soren N. Madsen of Caltech for NASA’s Jet Propulsion Laboratory. Further information is contained in a TSP (see page 1). NPO-43962



National Aeronautics and
Space Administration